Society for Mathematical Biology

CrossMark

The Impact of Recruitment on the Dynamics of an Immune-Suppressed Within-Human–Host Model of the *Plasmodium falciparum* Parasite

Woldegebriel A. Woldegerima[1,2] · **Miranda I. Teboh-Ewungkem**[3] · **Gideon A. Ngwa**[1]

Abstract A model is developed and used to study within-human malaria parasite dynamics. The model integrates actors involved in the development–progression of parasitemia, gametocytogenesis and mechanisms for immune response activation. Model analyses under immune suppression reveal different dynamical behaviours for different healthy red blood cell (HRBC) generation functions. Existence of a threshold parameter determines conditions for HRBCs depletion. Oscillatory dynamics reminiscent of malaria parasitemia are obtained. A dependence exists on the type of recruitment function used to generate HRBCs, with complexities observed for a more nonlinear function. An upper bound that delimits the size of feasible parasitized steady-state solution exists for a logistic function but not a constant function. The upper bound is completely characterized and is affected by parameters associated with HRBCs recruitment, parasitized red blood cells generation and the release and time-to-release of free merozoites. A stable density size for mature gametocytes, the bridge to invertebrate hosts, is derived.

Keywords Within-human–host dynamics · Innate and adaptive immune response · Parasitemia · Gametocytogenesis · Global stability · Red blood cells · Malaria · Recruitment

✉ Miranda I. Teboh-Ewungkem
ewungkems@gmail.com; mit703@lehigh.edu

1 Department of Mathematics, University of Buea, P.O. Box 63, Buea, Cameroon

2 African Institute for the Mathematical Sciences (AIMS) Cameroon, Limbe, Cameroon

3 Department of Mathematics, Lehigh University, Bethlehem, PA 18015, USA

1 Introduction and Background

Malaria remains one of the most prevalent and lethal human infections worldwide. It is also a significant problem in many tropical areas, especially in the Sub-Saharan African region of the world. Although, since 2000, malaria mortality rates have fallen among all age groups, including children under five (WHO 2015), the severity of the malaria problem is still a cause for concern. According to the WHO malaria report (2015), about 3.2 billion people remain at risk of malaria in 2015 alone, and there was an estimated 214 million new cases of malaria and 438,000 deaths, with 90% of cases in the sub-Saharan African countries.

Malaria is caused by a parasite of the genus *Plasmodium*. Of the five major species, *Plasmodium falciparum* is the most virulent and potentially lethal to humans. It is responsible for the greatest number of deaths and clinical cases and is the most widespread in the tropics (WHO 2015). Its infection can lead to serious complications affecting the brain, lungs, kidneys and other organs (Kirk 2001). It is our understanding that environmental factors such as sanitation; health factors including healthy eating habits, the availability of drugs and health facilities; climatic factors including global warming; social factors including civil disturbances, all influence the spread of malaria. Whatever the mitigating circumstances that favour the spread of malaria between (human) communities, the starting point for an index case is the development of the parasite within its (first) host (human and mosquito pair). It is now known that the malaria parasite has adapted its life cycle so that part of it is within the human host and the other part within the mosquito host. In this manuscript, we present a mathematical study of the within-human dynamics of the malaria parasite, taking into consideration the fact that in order to complete its life cycle, *Plasmodium* must move from mosquito to human and then back to mosquito again (Langhorne 2006; NIAID 2010).

Many mathematical models have been proposed to study the dynamics of spread of malaria between human and mosquito populations; see, for example, Ngonghala et al. (2012), Ngonghala et al. (2015) and references therein. The interaction between the malaria parasite and the human host involves a number of interactions that result in some forms of the parasite evading the human immune system. Since the stages of the malaria life cycle are complex, this allows the use of various immune evasion strategies by the malaria parasite and has major implications in the development of a vaccine for malaria endemic areas (Kirk 2001). Parasites undergo a complex life cycle: they sexually reproduce in mosquitoes (vectors) and asexually reproduce in vertebrate (human) hosts. Here, we are interested in the mathematical study of the within-human–host dynamics of *Plasmodium falciparum*, the most dangerous *Plasmodium* species.

The within-human part of the life cycle of the malaria parasite, particularly the *Plasmodium falciparum* species involves three main stages (Teboh-Ewungkem et al. 2013; Weekley and Smith 2013). These are exo-erythrocyte (or pre-erythrocyte) or liver stage, erythrocyte asexual stage (or merozoite blood stage), erythrocyte sexual stage (or gametocyte blood stage). The exo-erythrocyte stage or liver stage starts when sporozoites injected by an infected mosquito are carried by the circulating blood to the human's liver. Here, they infect liver cells, multiply develop into (Hepatic) schizonts, which then rupture releasing a load of free merozoites into the bloodstream. In the erythrocyte stage (within-human blood stream stage), the free merozoites invade and

infect the red blood cells or erythrocytes, or die out naturally, or are eliminated by the immune system. During this erythrocyte stage, the merozoites undergo simple asexual multiplication within the red blood cell breaking down the cell's haemoglobin into amino acids. Eventually, some of the infected red blood cells rupture, releasing toxins and more free merozoites into the blood stream. The free merozoites re-invade other uninfected erythrocytes, and the blood stage cycle repeats itself over and over. This onslaught and destruction of the red blood cell population causes anaemia and related illnesses and is potentially fatal if the process is allowed to continue unchecked. For a proportion of infected red blood cells, the merozoites within the cell commit towards development of gametocytes and instead of the infected red blood cell eventually bursting to release more merozoites; it differentiates to become gametocytes. These are *the sexual forms of the parasite that are infective to the mosquito vectors* (Kaushal et al. 1980; Talman et al. 2004). The invasion of human blood by the parasite and the subsequent action of destruction of the red blood cells takes place in the presence of the immune system (Bousema and Drakeley 2011; Cuomo et al. 2009; Eichner et al. 2001; Gardiner and Trenholme 2015; Kiszewski 2010; Kuehn and Pradel 2010; Perlmann and Troye-Blomberg 2002; Tavares 2013; Teboh-Ewungkem and Yuster 2010).

White blood cells (WBCs), also called *leukocytes*, are the cells of the immune system that are involved in protecting the body against diseases and foreign invaders in general. The normal white blood cell count in human beings is in the range 4000–11,000 white blood cells per microlitre of blood (Hollowell et al. 2005). All the forms of defence mechanisms that the body have constitute what we refer to here as the human's immune system. We consider in this manuscript that the immune system operates at two levels of performance: the *innate (non-specific) and adaptive (specific) immunity* levels. The innate immune system is the first line of defence against invading pathogens such as malaria parasites (Bousema et al. 2011; Janeway et al. 2001; Sompayrac 2015). The innate immune response mechanism relies on recognition of pathogens (such as the malaria parasite), as foreign bodies, to the system. On the other hand, the adaptive level of immunity relies on the ability of the system to switch into activity, by for example, using variable antigen-specific (or adaptive) receptors produced as a result of gene rearrangements and triggered by the presence or activity of the invading foreign organism. In contrast to innate immunity, the adaptive immune system acts as a second line of defence which also provides protection against re-invasion to the same parasites. It allows for a targeted response against a specific pathogen. Only vertebrates have specific immune responses (Bousema et al. 2011). An effective adaptive immune response normally comprises two pathways: antibody-mediated immunity and cell-mediated immunity that come into play at different stages of the attack by the foreign organism (Anderson et al. 1989; Aron 1988a; Augustine et al. 2009; Chiyaka et al. 2008; Langhorne et al. 2008; Li et al. 2011; Okrinya 2015; Perlmann and Troye-Blomberg 2002; Tumwiine et al. 2008). Here, for simplicity, we basically refer to the adaptive immune response without reference to its pathway to activation.

One of the most complex evolutionary adaptive features of the malaria parasite is the dynamic interaction between the parasite and the human's immunity. The parasite's action of destroying the red blood cells of the human can quickly overrun the human

system as toxins released from the parasite's metabolism and death cells residues accumulate leaving the human anaemic and poisoned. The onslaught during a first malaria attack is very severe as the human's system struggles to cope. Survival of the human during subsequent attacks depends very strongly on surviving the first malaria attack. It is therefore crucial that we understand the workings of the human immune system during a malaria attack. In general, once a human being is infected, then he/she starts developing acquired immunity (antibodies) that helps an individual to become (immune to) better capable of coping with malaria parasite load. It is now known that immunity to malaria is sustained by continuing exposure (Aron 1988a; Cowman et al. 2012; Cuomo et al. 2009; Gurarie et al. 2012; Perlmann and Troye-Blomberg 2002).

Mathematical models of the within-human–host dynamics of the malaria parasite play an important role in understanding the different developmental stages including the triggering gametocyte development as well as the interaction with the human immune system and even the pharmaco-kinetics of malaria drugs. The literature on within-human–host mathematical models for malaria parasite is vast (Anderson et al. 1989; Roy 1998; Bousema and Drakeley 2011; Heffernan 2011; Hetzel and Anderson 1996; Iggidr et al. 2006; Kuehn and Pradel 2010; Langhorne 2006; Perlmann and Troye-Blomberg 2002; Tavares 2013; Tewa et al. 2012; Wahlgren and Perlmann 1999; Weekley and Smith 2013; World Health Organisation 2010; Wongsrichanalai et al. 2007. Worthy of note are the works of Anderson, May, Gupta and others (Anderson et al. 1989; Roy 1998; Chiyaka et al. 2008; Li et al. 2011; Hellriegel 1992; Tewa et al. 2012; Tumwiine et al. 2008) that have significantly set the stage for these class of models. Some authors, such as Hoshen et al. (2000) and Iggidr et al. (2006), have extended these works without including immune system, while others such as Hoshen et al. (2000) have extended by including time-delay for the infected red blood cells. Still others have extended by considering the compartmental age stage developments of the infected red blood cells parasite based on a finite number of compartments, for example Bichara et al. (2012), Chiyaka et al. (2008), Gravenor and Kwiatkowski (1998), Gravenor and Lloyd (1998), Iggidr et al. (2006) and Wahlgren and Perlmann (1999).

In most of the works cited above, the concept of including immature and mature gametocytes and the interplay between the rate of generation of new healthy red blood cells and the general state of the system have been handled either partially or inadequately. Here, we present a comprehensive ordinary differential equation model that captures the different stages in the development of the parasite within the human body up to and including the generation of gametocytes and its interplay with the adaptive and innate immune state of the human. We study how the rate of generation of healthy red blood cells affects the state of the human host in a model system where healthy red blood cells, infected red blood cells, free merozoites, early-stage gametocytes, later-stage mature gametocytes, the innate and adaptive immune states of the systems are integrated into a single dynamical system. To the best of our knowledge, no such integrated model has been studied thus far. The rest of the manuscript is organized as follows: In Sect. 2, we present a complete formulation of the general model with immunity and establish the basic mathematical properties of boundedness, existence and uniqueness of solutions of the model. In Sect. 3, we re-parameterize, non-dimensionalizing the full model and in Sect. 4 carry out a careful and rigorous

study of a simple immune-suppressed model wherein the rate of generation of healthy red blood cells from the bone marrow is constant as well as the case for which the dynamics of generation of healthy erythrocytes is based on the Verhulst–Pearl logistic growth model. We present a numerical simulation or the model results based on realistic feasible parameter values as established in the literature, in Sect. 5 and then round up the manuscript with a discussion and conclusion in Sect. 6.

2 The Basic Mathematical Model

In a malaria-positive patient, the condition known as a malaria attack results from a system of interactions between the populations of mainly: (i) the healthy red blood cells (HRBCs), (ii) the human's infected red blood cells (IRBCs), (iii) the merozoites (that infect and destroy the red blood cells), (iv) the human's innate immune response, (v) the human's adaptive immune response (vi) the early-stage gametocyte and (vii) the late-stage gametocytes. The late-stage gametocytes are the forms of the malaria parasite that are infectious to mosquitoes. They are the transmissible forms of the parasite to mosquitoes and thus represent an important link to be included in the mathematical model analyses of the within-human dynamics of the malaria parasite. Thus, we shall use the seven compartments indicated as state variables to develop our model of the within-human–host dynamics of malaria parasite. To capture the immune response to malaria, we shall consider two types: adaptive immune response, simply assumed to be sustained by continuous exposure to the malarial infection, and innate immune response, the immune response that a human has in the natural state to clear foreign pathogens in the human's system. The innate immune status also affects the progression of the malarial infection within the human's system. As noted in the introduction, the model presented here generalizes previous works on the within-human dynamics of malaria parasites, for example, as in Anderson et al. (1989), Chiyaka et al. (2008), Hetzel and Anderson (1996), Li et al. (2011), Okrinya (2015) and Tewa et al. (2012). In particular, to the best of our knowledge, our mathematical model is probably the only ordinary differential equations within-host malaria model thus far that explicitly incorporates the late-state gametocytes, the actual transmissible and infectious forms of the parasites, as well as incorporates both the innate and adaptive immune effects in the model development. Most of the previous models combine both immune effects; however, the adaptive immune effects are only initiated due to continuous exposure and infection to the malaria parasite. Additionally, our study highlights the importance of the choice of HRBCs recruitment function indicating the complexity observed when a more nonlinear growth rate function is used to model the recruitment of healthy red blood cells. Most of the prior studies used the linear recruitment function, which is easier to analyse.

2.1 Description of the General Model Variables and Parameters

At any time t we assume that the human system comprises densities defined as follows: $R_h(t)$ healthy/unparasitized red blood cells (HRBCs), $R_p(t)$ parasitized/infected red blood cells (IRBCs), $M(t)$ free floating merozoites, $G_e(t)$ early/immature state game-

Table 1 Description of state variables and their quasi-dimension

State variable	Description	Quasi-dimension
R_h	Density of healthy red blood cells per unit volume	C
R_p	Density of infected red blood cells per unit volume	C
M	Density of merozoites per unit volume of blood	M
G_e	Density of immature gametocytes per unit volume	G
G_l	Density of mature gametocytes per unit volume	G
E_i	Density of innate immune system cells per unit volume	I
E_a	Density of adaptive immune system cells per unit volume	I

C = density of cells per unit volume of blood usually red blood cells per microlitre of blood; M = density of merozoites per unit volume of blood usually merozoites per microlitre of blood; G = density of Gametocytes per unit volume of blood usually gametocytes per microlitre of blood; I = density of immune system cells per unit volume, usually per microlitre of blood

tocytes, $G_l(t)$ late/mature state gametocytes, $E_a(t)$ adaptive immune system cells, $E_i(t)$ innate immune system cells. These seven types of cells interact in a specific way and the general state of the person will depend on the concentrations of these cell types in the system. We will adopt the following units: time is measured in days, volume in microlitre, μl, HRBCs and IRBCs are measured in cell density per unit volume, denoted C = Cell density $\times \mu l^{-1}$, free floating merozoites are measured in merozoite density per unit volume, denoted M = Merozoite density $\times \mu l^{-1}$, gametocytes, mature and immature are measured in gametocyte density per unit volume, denoted G = gametocyte density $\times \mu l^{-1}$, innate and adaptive immune cells are measured in immune cell density per unit volume, denoted I = immune cells $\times \mu l^{-1}$. Table 1 summarizes the state variables indicating their quasi-dimensions.

We now briefly describe how the equations governing the time rate of change of each of the entities in Table 1 are constructed. A summary of the parameters used through in the model equations is given in Table 2.

2.2 Derivation of the General Model Equations

(i) *The Healthy red blood cells (HRBCs), R_h* The density of healthy red blood cells is increased when the bone marrow produces more of these cells at the rate $\psi(R_h)$ per healthy red blood cell per time. We assume that the healthy red blood cells die naturally at rate $\mu_h > 0$ per healthy red blood cell. In addition, the density of healthy red blood cells is reduced when they are invaded and parasitized by free floating merozoites through simple mass action contact with contact parameter β_1. The equation governing the healthy red blood cell density takes the form:

$$\frac{dR_h}{dt} = R_h \psi(R_h) - \mu_h R_h - \frac{\beta_1 R_h M}{1 + \xi_0 E_a}, \tag{1}$$

Table 2 Description of parameters and their quasi- dimensional units

Parameter	Description	Quasi-dimension
β_1	Mass action contact parameter between free merozoites and healthy red blood cells. This parameter also models the effective rate of parasitization of healthy red blood cells by merozoites	$M^{-1}T^{-1}$
β_2	Adjusted mass action contact parameter between free merozoites and healthy red blood cells. It also models the effective absorption rate of free merozoites by red blood cells as the merozoites seek to enter the cells and being cleared as free merozoites from the blood stream	$C^{-1}T^{-1}$
β_3	Mass action contact parameter between free merozoites and infected red blood cells. It also models the effective absorption rate of free merozoites by infected red blood cells as the merozoites seek to enter the cells and being cleared as free merozoites from the blood stream	$C^{-1}T^{-1}$
Θ	Constant recruitment rate of healthy red blood cells from bone marrow	CT^{-1}
μ_h	Per capita natural death rate of healthy red blood cells	T^{-1}
$\tilde{\mu}_h$	Additional death of healthy red blood cells due to density-dependent related contact inhibition and other limiting processes	$C^{-1}T^{-1}$
Λ	Linear growth rate of red blood cells due to per capita production of red blood cells from the bone marrow	T^{-1}
μ_p	Per capita natural linear death rate of infected erythrocytes	T^{-1}
μ_e	Per capita natural linear death rate of immature gametocytes	T^{-1}
μ_l	Per capita natural linear death rate of mature gametocytes	T^{-1}
μ_m	Per capita natural linear death rate of freely floating merozoites	T^{-1}
μ_i	Per capita natural linear death rate of innate immune system cells	T^{-1}
μ_a	Per capita natural linear death rate of adaptive immune system cells	T^{-1}
δ_i	Linear growth rate of innate immune system cells	T^{-1}
K_i	Effective carrying capacity of the systems environment for innate immune system cells	I
M_i	Switching point for innate immune system cells below which the innate immunity becomes ineffective. Here $0 < M_i < K_i$	I

Table 2 continued

Parameter	Description	Quasi-dimension
ξ_0	The efficiency of the adaptive immune effectors in inhibiting merozoite contact with red blood cells via mass action contact	I^{-1}
ξ_1	The efficiency of the adaptive immune effectors in inhibiting merozoite transformation in parasitized red blood cells	I^{-1}
ξ_2	The efficiency of the adaptive immune effectors in inhibiting maturation of early-state gametocytes	I^{-1}
ρ_p	Mass action contact rate between parasitized red blood cells and innate immune system cells resulting in the elimination of the parasitized cells	$I^{-1}T^{-1}$
ρ_m	Mass action contact rate between free merozoites and innate immune system cells resulting in the elimination of the free merozoites	$I^{-1}T^{-1}$
ρ_g	Mass action contact rate between immature gametocytes and innate immune system cells resulting in the elimination of the immature gametocytes	$I^{-1}T^{-1}$
ρ_l	Mass action contact rate between mature gametocytes and innate immune system cells resulting in the elimination of the mature gametocytes	$I^{-1}T^{-1}$
ρ_a	Mass action contact rate between infected red blood cells, innate immune system cells and adaptive immune system cells. These are additional clearances due to the presence of adaptive immunity	$I^{-2}T^{-1}$
ρ_n	Mass action contact rate between merozoites, innate immune system cells and adaptive immune system cells. These are additional clearances due to the presence of adaptive immunity	$I^{-2}T^{-1}$
ρ_q	Mass action contact rate between immature gametocytes, innate immune system cells and adaptive immune system cells. These are additional clearances due to presence of adaptive immunity	$I^{-2}T^{-1}$
r	Average number of merozoites released by each bursting infected red blood cell	MC^{-1}
s	Average number of early-stage gametocytes arising from one infected red blood cell	GC^{-1}
σ	$\sigma \in [0, 1]$ is the proportion of the infected red blood cells that differentiate towards the path to gametocytogenesis	1
γ_p	Rate of maturation per infected red blood cell to a point where the IRBC either bursts to release more free merozoites or continue differentiating towards the gametocytogenesis path	T^{-1}

Table 2 continued

Parameter	Description	Quasi-dimension
γ_l	Rate of maturation per immature gametocyte to mature gametocytes	T^{-1}
ϑ_1	Linear response/production rate of innate immune effectors due to stimulation by infected red blood cells	$IC^{-1}T^{-1}$
ϑ_2	Linear response/production rate of adaptive immune effectors due to stimulation by free merozoites	$IM^{-1}T^{-1}$
ϱ_1	Linear response/proportion rate of adaptive immune system cells due to stimulation by parasitized red blood cells	$IC^{-1}T^{-1}$
ϱ_2	Linear response/proportion rate of adaptive immune system cells due to simulation by free merozoites	$IM^{-1}T^{-1}$
λ_1	Mass action contact parameter between infected red blood cells and innate immune system cells modelling the rate of depletion of the innate immune	$C^{-1}T^{-1}$
λ_2	Mass action contact parameter between free merozoites and innate immune system cells. This parameter is modelling the rate of depletion of the innate immunity due to such contact	$M^{-1}T^{-1}$
θ_1	Mass action contact parameter between infected red blood cells and adaptive immune system cells. This parameter is modelling the rate of depletion of the adaptive immunity through mass action contact	$C^{-1}T^{-1}$
θ_2	Mass action contact parameter between free merozoites and adaptive immune system cells. This parameter is modelling the rate of depletion of the adaptive immunity due to the contact	$M^{-1}T^{-1}$

where ξ_0 is a positive parameter measuring the efficiency of the adaptive immune cells E_a at prohibiting the destruction of the healthy red blood cells. As a function of R_h, the function $\psi : [0, \infty) \rightarrow \mathbb{R}$ is assumed to have the following properties:

(1) $\psi(0_+) > 0$, $\psi(R_h) \geq 0$, $\forall R_h \geq 0$, where $\psi(0_+) = \lim_{R_h \to 0+} \psi(R_h)$. This condition ensures that the quantity $R_h \psi(R_h)$ is non-negative and represents the net rate of production of new R_h per time.

(2) $\psi'(R_h) < 0$ $\forall R_h \geq 0$. This condition ensures that ψ is a continuously differentiable monotone decreasing function of its argument and that $R_h \psi(R_h)$ is bounded above with a maximum value given by $\hat{R}_h \psi(\hat{R}_h)$, where $\hat{R}_h \in [0, \infty)$ satisfies the equation $\psi(\hat{R}_h) + \hat{R}_h \psi'(\hat{R}_h) = 0$.

(3) $\lim_{R_h \to +\infty} \psi(R_h) \leq \psi(R_h) < \lim_{R_h \to 0+} \psi(R_h)$, $\forall R_h > 0$. This condition ensures that the equation $\dfrac{dR_h}{dt} = R_h \psi(R_h) - \mu_h R_h$ which represents the dynamics of healthy erythrocytes in the absence of infection has a nonzero steady-state solution R_h^* such that $R_h^* = \psi^{-1}(\mu_h)$ which is stable. Furthermore, it ensures the existence of a carrying capacity K such that for

$R_h < K$, $\dfrac{dR_h}{dt} > 0$ and thus the population R_h is increasing with time and for $R_h > K$, $\dfrac{dR_h}{dt} < 0$ and thus R_h is decreasing with time t. There are many choices of the function ψ which satisfies the above condition. In this manuscript, we consider two forms (see Ngonghala et al. (2016) and a brief discussion in "Appendix" for other function choices).

(a) $\psi(R_h) = \dfrac{\Theta}{R_h}$ so that in the absence of infection and immunity, the equation for the healthy red blood cells is modelled by the constant recruitment linear growth model in biology.

(b) In the second instance, we consider $\psi(R_h) = \Lambda - \tilde{\mu}_h R_h$ where Λ is the per capita constant recruitment rate of HRBCs from bone marrow and $\tilde{\mu}_h$ is additional death rate per HRBCs when we evoke the assumption that a self-limiting process kicks in for large densities, so that additional deaths are possible. In this case, the dynamics of HRBC in the absence of infection $R_h \psi(R_h) - \mu_h R_h$ will effectively be the logistic growth model in biology originally proposed by Verhulst (1838) and used by Pearl (1925). We note, however, that this form of ψ does not satisfy the positivity condition above when $R_h > \dfrac{\Lambda}{\mu_h}$, but we assume that, in this case, $\dfrac{\Lambda}{\mu_h}$ is sufficiently large and continue to use the postulated form for $\psi(R_h)$ for mathematical tractability.

(ii) *The Parasitized/Infected red blood cells (IRBC), R_p* Parasitized red blood cells are produced when free merozoites infect healthy red blood cells through mass action contact. They die naturally with linear death rate μ_p per parasitized red blood cells. The density of parasitized red blood cell reduces when the parasites in them change course at rate γ_p per infected red blood cell, developing and maturing to the point where they either burst to release more free merozoites into circulation or continue through the gametocytogenesis path towards formation of gametocytes. In addition, specific innate and adaptive immune responses remove infected red blood cells through mass action contact. The equation governing time rate of change of these class of cells takes the form

$$\frac{dR_p}{dt} = \frac{\beta_1 R_h M}{1 + \xi_0 E_a} - (\gamma_p + \mu_p) R_p - (\rho_p + \rho_a E_a) R_p E_i, \qquad (2)$$

where $\rho_p > 0$ and $\rho_a > 0$ are mass action contact terms that measure the efficiency of the immune system to clear the system of parasitized red blood cells.

(iii) *The free Merozoites, M* The density of free merozoites is increased when a fraction $(1 - \sigma)$ of the parasitized red blood cells rupture at rate γ_p releasing r merozoites per bursting red blood cell. They die naturally at rate μ_m per merozoite and are cleared from the system (both in the free and combined state) by both the adaptive and innate immune system. The time rate of change for the equation of the merozoites takes the form:

$$\frac{dM}{dt} = \frac{r \gamma_p (1 - \sigma) R_p}{1 + \xi_1 E_a} - \mu_m M$$

$$-\left(\frac{\beta_2 R_h}{1 + \xi_0 E_a} + \frac{\beta_3 R_p}{1 + \xi_0 E_a} + (\rho_m + \rho_n E_a) E_i\right) M, \tag{3}$$

where $\rho_m > 0$, $\rho_n > 0$, $\beta_2, \beta_3 > 0$ are mass action contact terms and ξ_1 is the efficiency of the adaptive immune effectors in inhibiting merozoite transformation in parasitized red blood cells. ξ_o is as described earlier.

(iv) *The early-state or immature gametocytes, G_e* The early-state gametocytes are produced from the fraction σ of the parasitized red blood cells that differentiate and mature at rate γ_p, following the gametocytogenesis path, leading to the production of s gametocytes per parasitized red blood cell of this type. They die naturally at rate μ_e per early-stage gametocyte. The density of this type of cells also reduces when the adaptive and innate immune system cells clear them through mass action contact and when the early-state gametocytes mature at rate γ_l to enter the late-stage gametocyte class. The time rate of change for the equation for the early-state or immature gametocytes takes the form:

$$\frac{dG_e}{dt} = \frac{s\sigma\gamma_p R_p}{1 + \xi_1 E_a} - (\gamma_l + \mu_e) G_e - (\rho_g + \rho_q E_a) E_i G_e, \tag{4}$$

where $\rho_g > 0$, $\rho_q > 0$ are mass action contact terms and ξ_1 is as described earlier.

(v) *The late-state or mature Gametocytes, G_l* The late-state gametocytes are formed when the early-state gametocytes mature at rate γ_l. They die naturally at rate μ_e per early-state gametocyte. The density of this type of cells is also reduced when the innate immune system cells clear them through mass action contact. The time rate of change for the equation for the early-state or mature gametocytes takes the form:

$$\frac{dG_l}{dt} = \frac{\gamma_l G_e}{1 + \xi_2 E_a} - \mu_l G_l - \rho_l E_i G_l, \tag{5}$$

where $\rho_l > 0$ is a mass action contact term. It is assumed that the adaptive immune system does not have an effect on the late-state gametocytes as the these are cloaked against them. However, it is believed to play a role in inhibiting the maturation of early-state gametocytes and the efficiency of this process is modelled via ξ_2.

(vi) *The Innate Immune system, E_i* The density of the innate immune system cells is maintained by the body at a rate $H_i(E_i)$, where $H_i : [0, \infty) \to \mathbb{R}$ is a continuously differentiable function of its argument. The innate immune system is also boosted by the presence of infection in the body and is depleted as they fight the infection since elimination of the foreign body in the system is assumed to be done by phagocytosis. The equation for the innate immune system takes the form

$$\frac{dE_i}{dt} = H_i(E_i) + \vartheta_1 R_p + \vartheta_2 M - (\lambda_1 R_p + \lambda_2 M) E_i, \tag{6}$$

where $\vartheta_1 > 0$, $\vartheta_2 > 0$, $\lambda_1 > 0$ and $\lambda_2 > 0$ are constant parameters as explained in Table 2. Here, $H_i : [0, \infty) \to \mathbb{R}$ is at least $\mathcal{C}^1-$ function. $H_i(E_i)$ can have different forms, but here we present two possible cases:

(a) In the first case, H_i is be modelled by the Verhulst–Pearl logistic model $H_i(E_i) = \delta_i E_i \left(1 - \frac{E_i}{K_i}\right)$, where $\delta_i > 0$ is the net linear per capita growth rate of innate immune system cells and $K_i > 0$ is the carrying capacity of the environment for innate immune system cells.

(b) In the second case, H_i it is modelled with a model that accounts for Allee effect, $H_i(E_i) = \delta_i E_i \left(1 - \frac{E_i}{K_i}\right)\left(\frac{E_i}{M_i} - 1\right)$, where δ_i and K_i retain their character as presented in (a), but $M_i > 0$ is a constant switch point immune system cell density, which is the Allee threshold density. At an innate immune density below M_i, innate immunity ceases to be effective. So, for this switch to be effective and meaningful, we assume that $0 < M_i < K_i$.

(vii) *The Adaptive Immune system, E_a* We assume that the adaptive immune system gets activated when the infection is in the system, and that it wanes over time in the absence of infection. The rate of change for the equation for the adaptive immunity takes the form

$$\frac{dE_a}{dt} = \varrho_1 R_p + \varrho_2 M - \left(\mu_a + \theta_1 R_p + \theta_2 M\right) E_a, \tag{7}$$

where ϱ_1, ϱ_2, θ_1, θ_2 and μ_a are positive constants each of whose interpretation is given in Table 2. It is clear in this formulation that in the absence of infection ($R_p = M = 0$, $\forall t > 0$), E_a will decay exponentially to zero with time according to the relation $E_a \propto \exp(-\mu_a t)$, where $\mu_a > 0$ is the per capita rate of waning of the adaptive immunity.

The system we study in this manuscript is thus the set of seven ordinary differential equations which when collected together is the system

$$\frac{dR_h}{dt} = R_h \psi(R_h) - \mu_h R_h - \frac{\beta_1 R_h M}{1 + \xi_0 E_a}; \tag{8}$$

$$\frac{dR_p}{dt} = \frac{\beta_1 R_h M}{1 + \xi_0 E_a} - (\gamma_p + \mu_p) R_p - (\rho_p + \rho_a E_a) R_p E_i; \tag{9}$$

$$\frac{dM}{dt} = \frac{r \gamma_p (1 - \sigma) R_p}{1 + \xi_1 E_a} - \mu_m M$$
$$- \left(\frac{\beta_2 R_h}{1 + \xi_0 E_a} + \frac{\beta_3 R_p}{1 + \xi_0 E_a} + (\rho_m + \rho_n E_a) E_i\right) M; \tag{10}$$

$$\frac{dG_e}{dt} = \frac{s \sigma \gamma_p R_p}{1 + \xi_1 E_a} - (\gamma_l + \mu_e) G_e - (\rho_g + \rho_q E_a) E_i G_e; \tag{11}$$

$$\frac{dG_l}{dt} = \frac{\gamma_l G_e}{1 + \xi_2 E_a} - \mu_l G_l - \rho_l E_i G_l; \tag{12}$$

$$\frac{dE_i}{dt} = H_i(E_i) + \vartheta_1 R_p + \vartheta_2 M - \left(\lambda_1 R_p + \lambda_2 M\right) E_i; \tag{13}$$

$$\frac{\mathrm{d}E_a}{\mathrm{d}t} = \varrho_1 R_p + \varrho_2 M - \left(\mu_a + \theta_1 R_p + \theta_2 M\right) E_a. \tag{14}$$

The system described by (8)–(14) requires a set of initial conditions to complete its formulation. One set of initial conditions could be

$$\left.\begin{array}{l} R_h(0) = R_{0h} > 0, \quad R_p(0) = 0, \quad M(0) = M_0 \geq 0, \\ G_e(0) = 0, \quad G_l(0) = 0, \quad E_i(0) = E_{0i} > 0, \quad E_a(0) = 0. \end{array}\right\} \tag{15}$$

Figure 1 shows the flow chart of the model in the absence of immunity. In the presence of immunity, the variable components that will be affected are the parasitized red blood cells (R_p), the free merozoites M and the early-state gametocytes (G_e), affected by both the innate and adaptive immune systems, and the late-state gametocytes (G_l), affected by the innate immune system.

2.3 Invariance, Positivity, Boundedness and Uniqueness

We start by establishing that in consonance with biological reality, since all the state variables and parameters in the system are non-negative, the solution will also remain
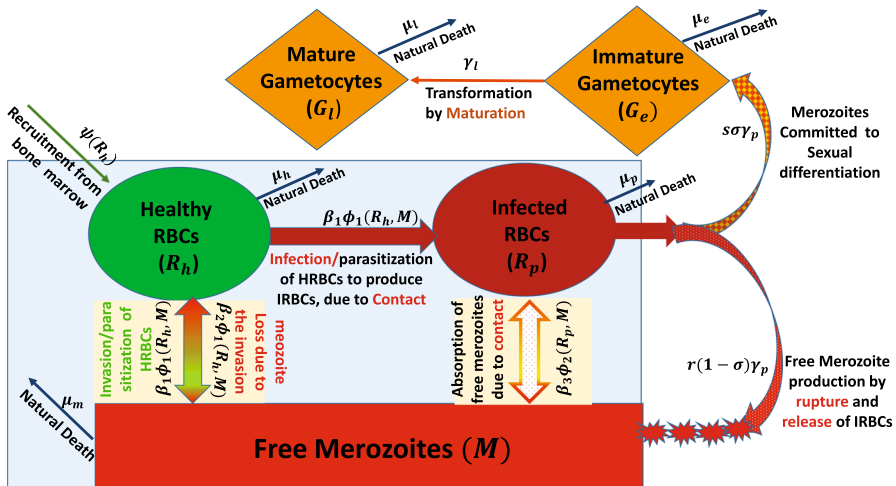

Fig. 1 Flow diagram showing the within-human–host dynamics of malaria parasite in the absence of immunity. Free merozoites (M) come in contact with HRBCs (R_h) modelled and illustrated by the function $\phi_1(R_h, M) = R_h M$, invading and infecting the HRBCs. This contact occurs at a mass action rate of β_1 to produce IRBCs (R_p). During this interaction, there is loss of merozoites as they are absorbed by the HRBCs, assumed to be at the contact rate β_2 to account for the fact that more than one merozoite may come in contact with a HRBC. The IRBCs either die naturally or mature following one of two paths at rate γ_p: a fraction σ follow the asexual path maturing to eventually rupture to produce r free merozoites per IRBC or follow the sexual path committed by the infecting merozoites to produce s early state/immature gametocytes (G_e) gametocytes, which will further mature to produce the late-state gametocytes (G_l). Free merozoites can also come in contact with IRBCs to be absorbed, modelled and illustrated by the function $\phi_2(R_p, M) = R_p M$, occurring at a mass action contact rate of β_3. Lastly death occurs from each parasite state at rate μ_{sub}, where sub represents the first letter of the class variable (Color figure online)

positive for all time. Let $\boldsymbol{x} = (R_h, R_p, M, G_e, G_l, E_i, E_a)^T$ be a column vector in $\mathbb{R}^7$, and define

$$\mathcal{S} = \left\{ \boldsymbol{x} \in \mathbb{R}^7 : R_h \geq 0, R_p \geq 0, M \geq 0, G_e \geq 0, G_l \geq 0, E_i \geq 0, E_a \geq 0 \right\} = \mathbb{R}^7_+.$$

We rewrite the dynamical system (8)–(14) with (15) in the form

$$\boldsymbol{x}' = \Phi(\boldsymbol{x}), \quad \boldsymbol{x}(0) = \boldsymbol{x}_0, \tag{16}$$

where $\Phi : \mathbb{R}^7 \times [0, \infty) \longrightarrow \mathbb{R}^7$ with $\Phi(\boldsymbol{x}) = (\phi_1, \cdots, \phi_7)^T (\boldsymbol{x})$ the vector valued function containing the RHS of the system as its components, $\boldsymbol{x}_0 = \left(R_{0h}, R_{0p}, M_0, G_{0e}, G_{0l}, E_{0i}, E_{0a} \right)^T$ is the column vector containing the initial conditions of the system, and T stands for the transpose. It is obvious that $\Phi \in \mathcal{C}^2$, that is, Φ is a twice continuously differentiable function since its components ϕ_i, $1 \leq i \leq 7$ are rational functions of the state variables, which are hypothesized to be $\mathcal{C}^2$.

Theorem 1 (Positivity and positive invariance of solution) *Consider system* (8)–(14) *with initial conditions in* (15) *and under the conditions given for* $\psi(R_h)$ *and* $H_i(E_i)$ *as stated in Sect.* 2.2. *Then, every solution of the system with initial condition in* $\mathbb{R}^7_+$ *remains in* $\mathbb{R}^7_+$. *Additionally, if* $\boldsymbol{x}(0) \equiv \boldsymbol{0}$, *the solution of system* (8)–(14) *will remain zero (or positively bounded depending on the form of* $\psi(R_h)$*), for all time* $t > 0$. *That is,* $\mathbb{R}^7_+$, *is positively invariant and attracting with respect to the system. Furthermore, the system has a forward positive solution in* $\mathbb{R}^7_+$ *provided that it starts in it.*

Proof See "Appendix" □

Theorem 2 (Boundedness of solution) *Consider system* (8)–(14) *with initial conditions in* (15) *and under the conditions for* $\psi(R_h)$ *and* $H_i(E_i)$ *as stated in Sect.* 2.2. *Then, every forward solution of the system in* $\mathbb{R}^7_+$, *with initial condition in* $\mathbb{R}^7_+$, *is bounded. Moreover, the system is uniformly dissipative in* $\mathbb{R}^7_+$.

Proof See "Appendix" □

Theorem 3 (Uniqueness of Solution) *The positive and bounded solution for the system* (8)–(14) *whenever it exists, is unique.*

Proof See "Appendix" □

3 Re-parameterization and Non-dimensionalization

In order to carry out mathematical analysis of our model, we start by scaling the model to reduce the number of relevant parameters. The only physical dimension in our system is that of time. But we have state variables which depend on the density of cells and parameters which depend on cell types and parasite densities. A state variable or parameter that measures the number of individuals of certain type has

dimension-like quantity associated with it (Ingemar 1985). To remove the dimension-like character on the parameters and variables, we make the following change of variables

$$r_h = \frac{R_h}{R_h^0}, \quad r_p = \frac{R_p}{R_p^0}, \quad m = \frac{M}{M^0}, \quad g_e = \frac{G_e}{G_e^0}, \quad g_l = \frac{G_l}{G_l^0},$$

$$e_i = \frac{E_i}{E_i^0}, \quad e_a = \frac{E_a}{E_a^0}, \quad \tau = \frac{t}{T^0} \tag{17}$$

where R_0^0, R_p^0, M^0, G_e^0, G_l^0, E_a^0 and E_i^0 are reference quantities associated with the different cell types and T^0 is a characteristic time frame for the system. In this regard, set

$$R_h^0 = R_p^0 = \begin{cases} \frac{\Theta}{\mu_h} & \text{if } \psi(R_h) = \frac{\Theta}{R_h} \\ \frac{\Lambda - \mu_h}{\tilde{\mu}_h} & \text{if } \psi(R_h) = \Lambda - \tilde{\mu}_h R_h, \end{cases}$$

$$M^0 = \frac{r\gamma_p}{\beta_2}, \quad G_e^0 = \frac{s\gamma_p R_p^0}{\mu_e + \gamma_l}, \quad G_l^0 = \frac{\gamma_l}{\mu_l} G_e^0, \quad E_i^0 = K_i, \quad E_a^0 = \varrho_1 R_p^0 T^0$$

and then define the dimensionless parameter groupings

$$T^0 = \frac{1}{\mu_p + \gamma_p}, \quad \beta = \frac{\beta_3}{\beta_2}, \quad \delta = \delta_i T^0, \quad K = \frac{M_i}{K_i},$$

$$a_0 = \begin{cases} \mu_h T^0 & \text{if } \psi(R_h) = \frac{\Theta}{R_h} \\ (\Lambda - \mu_h)T^0 & \text{if } \psi(R_h) = \Lambda - \tilde{\mu}_h R_h, \end{cases}$$

$$a_1 = \beta_1 M^0 T^0, \quad a_2 = \beta_2 R_h^0 T^0, \quad a_3 = \mu_m T^0,$$

$$a_4 = (\mu_e + \gamma_l)T^0, \quad a_5 = \mu_l T^0, \quad a_6 = \mu_a T^0,$$

$$\rho_1 = \rho_p E_i^0 T^0, \quad \rho_2 = \frac{\rho_a}{\rho_p} E_a^0, \quad \rho_3 = \rho_m E_i^0 T^0,$$

$$\rho_4 = \frac{\rho_n}{\rho_m} E_a^0, \quad \rho_5 = \rho_g E_i^0 T^0, \quad \rho_6 = \frac{\rho_q}{\rho_g} E_a^0,$$

$$\rho_7 = \rho_l E_i T^0, \quad p_0 = \xi_0 E_a^0, \quad p_1 = \xi_1 E_a^0, \quad p_2 = \xi_2 E_a^0,$$

$$b_1 = \frac{\vartheta_1 R_p^0 T^0}{E_i^0}, \quad b_2 = \frac{\vartheta_2 M^0}{\vartheta_1 R_p^0},$$

$$b_3 = \frac{\varrho_2 M^0}{\varrho_1 R_p^0}, \quad c_1 = \lambda_1 R_p^0 T^0, \quad c_2 = \frac{\lambda_2 M^0}{\lambda_1 R_p^0},$$

$$c_3 = \theta_1 R_P^0 T^0, \quad c_4 = \frac{\theta_2 M^0}{\theta_1 R_p^0}. \tag{18}$$

This leads to the scaled system

$$\frac{dr_h}{d\tau} = a_0 g(r_h) - \frac{a_1 m r_h}{1 + p_0 e_a}, \tag{19}$$

$$\frac{dr_p}{d\tau} = \frac{a_1 m r_h}{1 + p_0 e_a} - r_p - \rho_1 (1 + \rho_2 e_a) r_p e_i, \tag{20}$$

$$\frac{dm}{d\tau} = a_2 \left[\frac{(1 - \sigma) r_p}{1 + p_1 e_a} - m \left(\frac{r_h}{1 + p_0 e_a} + \frac{\beta r_p}{1 + p_0 e_a} \right) \right]$$
$$- a_3 m - \rho_3 (1 + \rho_4 e_a) e_i m, \tag{21}$$

$$\frac{dg_e}{d\tau} = a_4 \left[\frac{\sigma r_p}{1 + p_1 e_a} - g_e \right] - \rho_5 (1 + \rho_6 e_a) e_i g_e, \tag{22}$$

$$\frac{dg_l}{d\tau} = a_5 \left[\frac{g_e}{1 + p_2 e_a} - g_l \right] - \rho_7 e_i g_l, \tag{23}$$

$$\frac{de_i}{d\tau} = h(e_i) + b_1 (r_p + b_2 m) - c_1 (r_p + c_2 m) e_i, \tag{24}$$

$$\frac{de_a}{d\tau} = r_p + b_3 m - a_6 e_a - c_3 (r_p + c_4 m) e_a, \tag{25}$$

where

$$g(r_h) = \begin{cases} 1 - r_h & \text{if } \psi(R_h) = \frac{\Theta}{R_h} \\ r_h(1 - r_h) & \text{if } \psi(R_h) = \Lambda - \tilde{\mu}_h R_h \end{cases}, \tag{26}$$

$$h(e_i) = \begin{cases} \delta e_i(1 - e_i) & \text{if } H_i(E_i) = \delta_i E_i \left(1 - \frac{E_i}{K_i}\right) \\ \delta e_i(1 - e_i)(\frac{e_i}{K} - 1) & \text{if } H_i(E_i) = \delta_i E_i \left(1 - \frac{E_i}{K_i}\right) \left(\frac{E_i}{M_i} - 1\right) \end{cases} \tag{27}$$

From the definition of the parameters (Table 2), $0 < M_i < K_i \Rightarrow 0 < K < 1$, so that in the second case of (27), K is the innate immunity threshold below which the the innate immune effect becomes less effective. It is worth noting that to account for the reduced elimination of IRBCs by immune cells E_i and E_a, compared to their effect on free floating merozoites (Okrinya 2015), we should have: $\varrho_1 \leq \varrho_2$, $\theta_1 \leq \theta_2$, $\vartheta_1 \leq \vartheta_2$ and $\lambda_1 \leq \lambda_2$.

4 Model Analysis Under Immunity Suppression

In this section, we present the mathematical analysis of our model when both the innate and adaptive immunity are suppressed. We believe that to understand the role immunity plays on the within human–host *Plasmodium falciparum* dynamics, it is important to first understand how the function choice used to model recruitment of HRBCs impacts the model dynamics. Thus, we shall attempt an analysis subject to simplifications whereby in system (19)–(25), $e_i = e_a = 0$, that is, when immunity is suppressed, and for two choice functions for the net rate of production of HRBCs, given by the scaled function $g(r_h)$ and as defined by (26). With this simplification, system (19)–(25) reduces to the system,

$$\frac{dr_h}{d\tau} = a_0 g(r_h) - a_1 m r_h, \tag{28}$$

$$\frac{dr_p}{d\tau} = a_1 m r_h - r_p, \tag{29}$$

$$\frac{\mathrm{d}m}{\mathrm{d}\tau} = a_2 \left[(1 - \sigma) r_p - m \left(r_h + \beta r_p \right) \right] - a_3 m, \tag{30}$$

$$\frac{\mathrm{d}g_e}{\mathrm{d}\tau} = a_4 \left[\sigma r_p - g_e \right], \tag{31}$$

$$\frac{\mathrm{d}g_l}{\mathrm{d}\tau} = a_5 \left[g_e - g_l \right], \tag{32}$$

where the scaled parameters are as described in (18). For this simplified system, theorems 1, 2 and 3 still hold, with the bounds obtained by setting $e_i = e_a = 0$.

4.1 Parameters and Relative Sizes of the Scaled Parameters

Values used to quantify the parameters in Table 2 that pertains to the system (28)–(32) are either obtained from the literature or estimated using published biological information about the within-host malaria parasite dynamics. In particular, it is reported that the maximal natural life expectancy of human HRBCs is 120 days with very slight variations reported (Gottlieb et al. 2012; Sackmann 1995; Shemin and Rittenberg 1946). Thus, the per capita natural death rate of HRBCs, μ_h, is the reciprocal 1/120 per day. This value was also used in Anderson et al. (1989) and Li et al. (2011). Note, however, that a recent study (An et al. 2016) used a mathematical model to estimate this life span of HRBCs in humans for different age groups and gender, and they reported a range of 100–133 for humans aged 14 years and older. The range was lower, 54–85 days for children under 14 years (An et al. 2016).

IRBCs, on the other hand, change forms as the parasites in them mature, undergoing schizogony following the path to its immediate demise via the rupture and release of free floating merozoites or the path towards gametocyte formation. This rate γ_p is the reciprocal of the time period of schizogony and is faster (see Ginsburg and Hoshen (2002)) than the per capita natural death rate of HRBCs, i.e. $\mu_h < \gamma_p$. In particular, the schizogony time frame $1/\gamma_p$ takes about 48–72 h (i.e. $\approx$2–3 days), (Anderson et al. 1989; Baron 1996; Hoffman and Crutcher 2017; Ginsburg and Stein 1987) giving a range of 0.33–0.5 for γ_p. The process of schizogony ends with the release of r merozoites per bursting IRBC, where r has been reported (see Hetzel and Anderson (1996) and McKenzie and Bossert (1997)) to be in the range 8–32 for *plasmodium falciparum*, with a value of 36 also reported (Hoffman and Crutcher 2017).

Although most deaths of IRBCs that do not follow the path to gametocytogenesis are due to the rupture and release of merozoites, we assume here that any that do not rupture nor transform to immature or early-state gametocytes will be removed at the rate μ_p, assumed to be of the same order of magnitude as μ_h, if not slightly bigger (a value of 0.055 was cited in Okrinya (2015)), due to its parasitized state. Thus, $\mu_h \leq \mu_p \leq \mu_p + \gamma_p$. Next, *Plasmodium falciparum* free floating merozoites have a short life-span of less than 30 minutes (Hetzel and Anderson 1996; Talman et al. 2004 with other authors giving less than 20 minutes (Anderson et al. 1989). Thus, μ_m, the per capita linear death rate falls approximately in the range 48–72 per day. In terms of the scaled parameters (see Eq. (18)), we see that $a_3 = \mu_m T^0 = \frac{\mu_m}{\mu_p + \gamma_p} > 1$.

The recruitment parameters Θ and Λ are particular to the form of birth rate function used. For a constant recruitment rate of HRBCs from the bone marrow, $R_h \psi(R_h) = \Theta$ and the dynamics of the HRBC population in the absence of parasitemia is modelled by the constant recruitment linear death model $\frac{dR_h}{dt} = R_h \psi(R_h) - \mu_h R_h = \Theta - \mu_h R_h$. Values for Θ are estimated to be in the order of $10^4 - 10^7 \mu L$, estimated as follows: the number of new erythrocytes produced per second in a human is approximately 2.4 million (yielding $2.4 \times 10^6 \times 24 \times 3600$ per day) (Sackmann 1995). An adult human at about 150 lb has a volume of blood of about 4.5–5 litres, and this value depends on the gender and increases with weight. (Blood volume can be calculated using MedScape Blood volume Calculator.) This volume can go as low as about 1.47 litres for a 50 lb female. Thus, a range of $4 \times 10^4 - 6 \times 10^7$ cells per μL per day for adults, as cited in Bianconi et al. (2013), Hetzel and Anderson (1996) and Li et al. (2011), is not unreasonable. However, a more reasonable range in children should be reduced by about 30%.

For a density-dependent growth function, $R_h \psi(R_h) = (\Lambda - \tilde{\mu}_h R_h) R_h$. In this case, the HRBC population dynamics in the absence of parasitemia is modelled by the logistic growth model $\frac{dR_h}{dt} = R_h \psi(R_h) - \mu_h R_h = (\Lambda - \mu_h) R_h - \tilde{\mu}_h R_h^2$, where Λ is the per capita constant recruitment rate of HRBCs from bone marrow and $\tilde{\mu}_h$ is additional death rate per HRBCs when the assumption that a self-limiting process kicks in for large densities is evoked, so that additional deaths are possible (see Landaw (1987) and Willekens et al. (2008). The size of the limiting HRBC population is $\frac{(\Lambda - \mu_h)}{\tilde{\mu}_h}$. We estimate the recruitment term $\Lambda - \mu_h$ by considering the time period for a healthy adult person to replenish their blood after a blood donation. Based on the literature, when an adult donates blood the amount given is a pint representing about 10% of the individual's total blood volume (Brookhaven 2017). Most of the composition of blood dran from a donor is water with about just a third red blood cells. Iron is also lost in the process. Assuming a donor adheres to the guidelines of drinking plenty of fluids after a blood donation, it takes about a day to replenish the lost water but requires about 3 to 4 weeks to replace the lost blood and about 8 weeks to replace the iron lost (Brookhaven 2017). Thus, we estimate that the time from donation to full recovery is anywhere from a day to 66 days though a more reasonable time frame should be from about 2 days to 28 days. We estimate a baseline value of 4 days, to capture our guess that the initial replenishment period for the blood, after the water has been replenished, should be faster saturating as the time of 28 days is approached. Thus, based on these estimates, we estimate the rate $\Lambda - \mu_h$ to be in the range $\frac{1}{28} - \frac{1}{2}$ (yielding 0.036–0.5 per day). The maximal red blood cell count is of the order of $10^6 - 10^7$ cells per μL of blood [estimated from the total which is of the order of $10^{12} - 10^{13}$ in the entire blood volume of about 4.5–5 litres) (Bianconi et al. 2013; Sackmann 1995)].[1] Using this as an estimate for the limiting HRBC population size, $\frac{(\Lambda - \mu_h)}{\tilde{\mu}_h}$, we see that $3.6 \times 10^{-9} - 5.0 \times 10^{-7}$ is an estimated range for $\tilde{\mu}_h$.

---

[1] Note that the estimate in Bianconi et al. (2013) was for total cell count. However, the given range can be deduced based on the percentage of cells that are HRBCs.

Based on the above discussion, we now provide an estimate for the size of the scaled parameter a_0, which will depend on the non-dimensional growth function $g(r_h)$. For the linear growth function, $g(r_h) = (1 - r_h)$ with $a_0 = \mu_h T^0 = \frac{\mu_h}{\mu_p + \gamma_p} < 1$ since $\mu_h \leq \mu_p < \mu_p + \gamma_p$. For the logistic growth function, $g(r_h) = r_h(1 - r_h)$ with $a_0 = (\Lambda - \mu_h)T^0 = \frac{\Lambda - \mu_h}{\mu_p + \gamma_p}$. For this case, the value of a_0 could be less than or greater than unity depending on the net recruitment rate or HRBCs and so we can only state that $a_0 > 0$.

As earlier mentioned, some IRBCs do not rupture but continue the gametocytogenesis path, obligating the continuation of the malaria parasite life cycle. The proportion of merozoites that commit to gametocytes via gametocytogenesis, σ, is much smaller than the proportion that continue the schizogony path. Proportions of less than 10% (Josling and Llinás 2015; Julius et al. 2017) have been reported with a value of 6.4×10^{-3} used in Okrinya (2015). Gametocyte development is within an erythrocyte and erythrocytes that have male or females present are the potential contributors to the parasite forms in the mosquitoes after fertilization, if ingested by the mosquito (Teboh-Ewungkem and Wang 2012; Teboh-Ewungkem and Yuster 2010, 2016). The number of mature gametocytes, s, per infected red blood cell is either 0 or 1.

The maturation period for *Plasmodium falciparum* gametocyte takes approximately $10 - 12$ days (Josling and Llinás 2015; Julius et al. 2017; Sinden 1982). We break this up to account for early-state gametocytes (where the differentiation of state commences post the schizogony period, so stages II or III–IV) and the late-state gametocytes (stage V). Based on the chart in Bousema et al. (2011) and Talman et al. (2004), we assume that $1/\gamma_l$ is the maturation time frame from the period after schizogony to the mature state gametocytes, and we approximate this in the range 3–9 days and thus a range of 0.11–0.33 for γ_l. We note that this rate will depend on other intrinsic human factors. However, the smaller the rate, the longer it takes for gametocytes to mature, the better for control as gametocytes are the transmissible forms of the malaria parasite and a delay in the formation of these transmissible forms (the mature forms) translates to their inaccessibility and minimizes the chances of transmission.

The half-life for mature gametocytes is 2.4 days which can be used to estimate the death rate of mature gametocytes μ_l, as 0.28 per day. However, some gametocytes have been known to stay as long as four weeks in the bloodstream (Talman et al. 2004). In Okrinya (2015), a value of 0.02 per day was utilized; thus, a range of 0.02–0.28 per day for μ_l would be assumed. For early-state gametocytes, most of their loss comes from transformation into mature state gametocytes. However, we assume, here, that those that do not fully transform can be removed at a rate of maximum order as that mature state gametocytes. Given the size of μ_m, it is clear that $\mu_e < \mu_m$, $\mu_l < \mu_m$. Thus, $a_4 = (\mu_e + \gamma_l)T^0 = \frac{\mu_e + \gamma_l}{\mu_p + \gamma_p} < a_3$ and $a_5 = \mu_l T^0 = \frac{\mu_l}{\mu_p + \gamma_p} < a_3$.

The parameters with minimal experimental measurements and information are the mass action contact rates β_1, β_2, β_3. The rate β_1 models the effective parasitization of healthy red blood cells by merozoites. The size of its value determines the parasite's ability to invade and infect HRBCs, an obligate part of the parasites life cycle. It would play a significant role in initiating an immune response. Values for β_1 under immune suppression were estimated using a rat model for the parasite *Plasmodium berghei* in Hetzel and Anderson (1996) was 2×10^{-5}μL per cell per day. (The data were

reported in millilitres.) We do not expect these estimates to be same in humans and for *Plasmodium falciparum* parasite. However, it gives an idea of the order of magnitude of the contact rate. In Okrinya (2015), a value of $4.9 \times 10^{-6} \mu L$ per cell per day was used. Starting with this value, we will consider rates much higher and much less to ensure that the parasite ratios are of the right orders observed *in vivo*. Moreover, small values of β_1 are desirable for control purposes as they determine the parasite's ability to invade HRBCs. Thus, the effect of small values will be investigated as well.

As merozoites invade HRBCs, they are absorbed in the process as they seek to enter the cell, and thus cleared by the bloodstream in the process. We model this by the rate β_2. In Okrinya (2015) and Tewa et al. (2012), $\beta_1 = \beta_2$. Here, however, we assume that this rate is at most β_1, to account for the possibility of a reduction in absorption of free merozoites during the invasion of HRBCs, which may be a result of immune response. For the immune-suppressed model, we will consider that they are the same. Additionally, as in Hetzel and Anderson (1996) and Tewa et al. (2012) we assume that IRBCs can also absorb free merozoites; however, one would expect this rate to be no more than the rate β_2 as this is not an evolutionary productive way for the malaria parasite to ensure the successful completion of its life cycle. Thus, $\beta_3 \leq \beta_2 \leq \beta_1$ which account for a possibly smaller absorption effect, smaller by IRBCs compared to HRBCs, than parasitization contact.

From the scaling (18), we see that $a_1 = \beta_1 M^0 T^0 = \frac{\beta_1 r \gamma_p}{\beta_2(\mu_p + \gamma_p)} < \frac{\beta_1}{\beta_2} r$, which gives an upper bound for a_1. Since $\beta_3 \leq \beta_2 \leq \beta_1$, we can deduce that $\beta = \frac{\beta_3}{\beta_2} \leq 1$. Next, the scaled parameter $a_2 = \beta_2 R_h^0 T^0$ takes two forms depending on the choice of the birth rate $g(r_h)$. For $g(r_h) = (1 - r_h)$, $a_2 = \beta_2 R_h^0 T^0 = \frac{\beta_2 \Theta}{\mu_h(\mu_p + \gamma_p)} > 0$. However, for $g(r_h) = r_h(1 - r_h)$, $a_2 = \beta_2 R_h^0 T^0 = \frac{\beta_2(\Lambda - \mu_h)}{\mu_h(\mu_p + \gamma_p)} > 0$.

In summary, we have that

$$a_0 = \begin{cases} \frac{\mu_h}{\mu_p + \gamma_p} < 1 & \text{if } g(r_h) = 1 - r_h \\ \frac{\Lambda - \mu_h}{\mu_p + \gamma_p} > 0 & \text{if } g(r_h) = (1 - r_h) r_h \end{cases}, \quad 0 \leq a_1 < \frac{\beta_1}{\beta_2} r, \ a_2 > 0, \ a_3 > 1, \ 0 < a_4, a_5 < a_3.$$

$$(33)$$

Table 3 gives the values and range of values of the parameters used in the immune-suppressed model simulations.

In terms of the scaling (18), the scaled time $\frac{1}{\mu_p + \gamma_p}$ is the average life of a parasitized red blood cell until natural death or transformation to early-state gametocytes or rupture to release free floating merozoites. From a control perspective, if the bursting rate of IRBCs γ_p is greater than the per capita death rate μ_p, then IRBCs will burst releasing merozoites before they can be cleared, ensuring the continuation of parasitemia detrimental to patients with naive-immunity. However, if this fails, the propensity for the IRBCs to die before bursting is higher, a desirable outcome for a patient. Thus, for some parameter choices for the other variables, if $\mu_p < \gamma_p$ we could control parasitemia and if $\mu_p > \gamma_p$, then we would have persistence of parasitemia.

Table 3 Parameter values, their range, baseline values, units and citation

Parameter	Range of possible values	Baseline value	Units	Reference
β_1	$[10^{-10}, 10^{-5}]$	6.5×10^{-7}, 6.0×10^{-6}	μl/Cell day^{-1}	Okrinya (2015)
β_2	$\phi_1 \beta_1$, $0 \leq \phi_1 \leq 1$	$\phi_1 = 1$	μl/Cell day^{-1}	Tewa et al. (2012)
β_3	$\phi_2 \beta_2$, $0 \leq \phi_2 \leq 1$	$\phi_2 = 0.75$	μl/Cell day^{-1}	Estimated
Θ	$[4 \times 10^4, 6 \times 10^7]$	4.15×10^4	Cells/μl day^{-1}	Bianconi et al. (2013) and Hetzel and Anderson (1996); Li et al. (2011)
μ_h	$[\frac{1}{120}, \frac{1}{100}]$	$\frac{1}{120}$	day^{-1}	An et al. (2016), Anderson et al. (1989) and Li et al. (2011)
$\tilde{\mu}_h$	$[3.6 \times 10^{-9}, 5.0 \times 10^{-7}]$	5×10^{-8}	day^{-1}	Estimated
$\omega = \Lambda - \mu_h$	$[0.036, 0.5]$	0.25	day^{-1}	Estimated
μ_p	$[\frac{1}{120}, \frac{1}{5}]$	0.0091, 0.07	day^{-1}	Estimated
γ_p	$[0.33, 0.5]$	0.5	day^{-1}	Anderson et al. (1989), Hoffman and Crutcher (2017) and Ginsburg and Stein (1987)
μ_l	$[0.02, 0.28]$	0.28	day^{-1}	Talman et al. (2004) and Okrinya (2015)
μ_e	$[0.02, 0.28]$	0.28	day^{-1}	Estimated
μ_m	$[24, 72]$	48	day^{-1}	Anderson et al. (1989), Hetzel and Anderson (1996) and Talman et al. (2004)
r	$[8, 36]$	16	1	Anderson et al. (1989), Hoffman and Crutcher (2017), Hetzel and Anderson (1996) and McKenzie and Bossert (1997)
s	$0, 1$	1	1	Julius et al. (2017)
σ	$[0, 0.1]$	0.1, 0.0064	1	Josling and Llinás (2015), Julius et al. (2017) and Okrinya (2015)
γ_l	$[0.11, 0.33]$	0.15	day^{-1}	Bousema et al. (2011), Josling and Llinás (2015) and Talman et al. (2004)

C represents cells

4.2 Existence and Stability of Steady-State Solutions

We now examine the different special cases of the model for existence and stability of steady-state solutions.

4.2.1 Existence of Steady States

Theorem 4 *The immune-suppressed system described by the scaled Eqs.* (28)–(32) *has at least one steady-state solution whose existence, depending on its nature, depends on the size of a threshold parameter* $R_0 = \frac{a_1 a_2 (1-\sigma)}{a_2 + a_3}$. *In particular,*

1. *for $g(r_h) = 1 - r_h$, the system has a merozoite-free (or parasite-free) steady-state solution $x_{pf} = (1, 0, 0, 0, 0)$, which always exists for all values of R_0, and a non-trivial parasitized steady state, $x_e = (r_h^*, r_p^*, m^*, g_e^*, g_l^*) \in \mathbb{R}_+^5$, which only exists for $R_0 > 1$.*

2. *for $g(r_h) = r_h(1 - r_h)$, the system has a trivial steady-state solution $x_0 = (0, 0, 0, 0, 0)$, and a merozoite-free (or parasite-free) steady-state solution $x_{pf} = (1, 0, 0, 0, 0)$, both of which always coexists for all values of R_0, in addition to either zero, one or at most two positive merozoite steady-state solutions (m^*) that may result in either zero or one real positive parasitized steady-state solution (x_e) depending on the size of R_0 and*

$$0 < m^* < \frac{a_0}{a_1} \text{ so that } 0 < r_h^* < 1. \tag{34}$$

In particular,
   (a) *if $R_0 = 1$ there is a unique real positive merozoite steady-state solution for m^*, but it does not yield a real positive parasitized equilibrium solution within the bounds* (34)*;*
   (b) *if $R_0 < 1$ there is a unique real positive merozoite steady state solution for m^*, but it does not yield a real positive parasitized equilibrium solution within the bounds* (34)*;*
   (c) *if $R_0 > 1$, there are two real positive merozoite steady-state solutions for m^*, but only one leads to a unique real positive parasitized equilibrium solution within the bounds* (34)*.*
   The non-trivial positive parasitized steady state, when it exists, also always coexists with the trivial and parasite-free steady states.

Proof Let $(r_h^*, r_p^*, m^*, g_e^*, g_l^*)$ be a steady-state solution. Then, their values are obtained by solving the algebraic equations obtained by setting the right hand side of (28)–(32) to zero. Now, we have the following cases:
(i) $g(r_h) = 1 - r_h$. In this case, we have on solving the algebraic equations that

$$r_h^*(m^*) = \frac{a_0}{a_0 + a_1 m^*}, \quad r_p^*(m^*) = a_1 m^* r_h^*(m^*),$$
$$g_e^*(m^*) = \sigma r_p^*(m^*), \quad g_l^*(m^*) = g_e^*(m^*). \tag{35}$$

Substituting these in (30), and rearranging we have

$$\frac{m^* \left[a_0(a_2 + a_3)(R_0 - 1) - a_1(a_3 + \beta a_0 a_2)m^* \right]}{a_0 + a_1 m^*} = 0$$

leading to the two solutions

$$m^* = 0 \quad \text{or} \quad m^* = \frac{a_0(a_2 + a_3)(R_0 - 1)}{a_1(a_3 + \beta a_0 a_2)}, \tag{36}$$

where

$$R_0 = \frac{a_1 a_2 (1 - \sigma)}{a_2 + a_3}. \tag{37}$$

Observe that the nonzero solution for m^* in (36) exists and is positive only when $R_0 > 1$ and that when $R_0 \leq 1$ the only steady-state solution for which each of the variables in (35) is non-negative is the parasite-free solution $(r_h^*, r_p^*, m^*, g_e^*, g_l^*) = x_{pf} = (1, 0, 0, 0, 0)$. Moreover, when $R_0 > 1$, a steady state solution $x_e = (r_h^*, r_p^*, m^*, g_e^*, g_l^*)$, for which all the state variables are positive is given by (35) with explicit form obtained by substituting m^* given in (36) into Eq. (35) yielding

$$r_h^* = \frac{a_3 + \beta a_0 a_2}{a_3 + \beta a_0 a_2 + (a_2 + a_3)(R_0 - 1)}, \quad r_p^* = \frac{a_0(a_2 + a_3)(R_0 - 1)}{a_3 + \beta a_0 a_2 + (a_2 + a_3)(R_0 - 1)},$$
$$g_e^* = g_l^* = \sigma r_p^* = \frac{\sigma a_0(a_2 + a_3)(R_0 - 1)}{a_3 + \beta a_0 a_2 + (a_2 + a_3)(R_0 - 1)}. \tag{38}$$

This establishes the proof of the first part of the theorem.

(ii) $g(r_h) = r_h(1 - r_h)$. In this case, the algebraic equations are no longer linear functions, but the steady-state solution, $x_0 = (0, 0, 0, 0, 0)$, that is the steady state where both the merozoite and red blood cell densities are at the trivial state and the merozoite-free or disease-free steady state, $x_{pf} = (1, 0, 0, 0, 0)$ are easily obtained. The steady-state solution, where both the merozoite and healthy red blood cell densities are nonzero, denoted by $x_e = (r_h^*, r_p^*, m^*, g_e^*, g_l^*)$ is now defined by

$$r_h^*(m^*) = \frac{a_0 - a_1 m^*}{a_0}, \quad r_p^*(m^*) = a_1 m^* r_h^*(m^*), \quad g_l^*(m^*) = g_e^*(m^*) = \sigma r_p^*(m^*),$$
$$\tag{39}$$

where m^* is the positive solution of the quadratic equation

$$m^{*2} - C_1 m^* + C_0 = 0. \tag{40}$$

Solving Eq. (40) yields two possible solutions, m_1^* and m_2^*, of m^*, defined as

$$m_1^* = \frac{1}{2} \left(C_1 - \sqrt{C_1^2 - 4C_0} \right), \quad \text{and} \quad m_2^* = \frac{1}{2} \left(C_1 + \sqrt{C_1^2 - 4C_0} \right) \tag{41}$$

where

$$C_1 = \frac{a_2\left(a_0\beta + (R_0 - 1)\right) + a_3 R_0}{a_1 a_2 \beta}, \quad C_0 = \frac{a_0\left(a_2 + a_3\right)\left(R_0 - 1\right)}{a_1^2 a_2 \beta}, \qquad (42)$$

with R_0 as defined in (36). For any R_0 value, the solutions of (41), m_1^*, m_2^* could produce zero, one or two positive real solutions depending on whether $C_1^2 - 4C_0 \geq 0$ or not. Observe that

$$C_1^2 - 4C_0 = D_2\left(R_0^2 - D_1 R_0 + D_0\right) = D_2\left(\left(R_0 - \frac{D_1}{2}\right)^2 - \frac{D_1^2 - 4D_0}{4}\right),$$

$$(43)$$

where $D_0 = \frac{a_2\left(a_2(a_0\beta+1)^2 + 4a_0 a_3 \beta\right)}{(a_2+a_3)^2} > 0$, $D_1 = \frac{2a_2(a_0\beta+1)}{a_2+a_3} > 0$, $D_2 = \frac{(a_2+a_3)^2}{a_1^2 a_2^2 \beta^2} > 0$ and $D_1^2 - 4D_0 = -\frac{16a_0 a_2 a_3 \beta}{(a_2+a_3)^2} < 0$, showing that there are no real values of R_0 for which $C_1^2 - 4C_0 = 0$, nor $C_1^2 - 4C_0 < 0$ since $C_1^2 - 4C_0$ is a continuous function of R_0. Thus, the solutions of (41) are real.

Specifically, if $R_0 = 1$, $C_0 = 0$ and the solutions to (40) are $m^* = 0$ and $m^* = C_1$. The solution $m^* = 0$ produces the parasite-free steady state $\boldsymbol{x}_{pf} = (1, 0, 0, 0, 0)$, while the solution $m^* = C_1$ at $R_0 = 1$ reduces to $m^* = \frac{a_0 a_2 \beta + a_3}{a_1 a_2 \beta} > \frac{a_0}{a_1}$, making the steady-state variable, $r_h^*(m^*)$ defined by (39), to fall outside the bounds of Eq. (34) and hence unrealistic in the context of the scaling in this manuscript. Thus, there is no positive parasitized steady-state solution, only the trivial and parasite-free steady states. This establishes the proof of part (a) of the second part of the theorem.

If $R_0 < 1$, $C_0 < 0$ and from (41), $\sqrt{C_1^2 - 4C_0} > |C_1|$, which implies that $m_1^* < 0$ and $m_2^* > 0$, regardless of the sign of C_1. Thus, only one positive solution of m^* exists for $R_0 < 1$ and it is $m^* = m_2^*$ which is greater than C_1. However, for the parasitized steady state $\boldsymbol{x}_e = (r_h^*, r_p^*, m^*, g_e^*, g_l^*)$, to exist in $\mathbb{R}_+^5$, the restrictions in (34) must hold, that is m_2^* must lie in $(0, \frac{a_0}{a_1})$. We next prove that m_2^* as defined in (41) falls outside the interval $(0, \frac{a_0}{a_1})$. First, notice that C_1 in Eq. (42) can be rewritten as

$$C_1 = \frac{a_0}{a_1} + \frac{(a_2 + a_3)}{a_2 a_1 \beta}\left(R_0 - \frac{a_2}{(a_2 + a_3)}\right) = \frac{a_0}{a_1} + \frac{a_1(1 - \sigma) - 1}{a_1 \beta}. \qquad (44)$$

It is worth observing that for $\frac{a_2}{a_2+a_3} \leq R_0 < 1$, $C_1 \geq \frac{a_0}{a_1} > 0$ and so $m_2^* \geq \frac{a_0}{a_1}$. Next, we easily establish by implicit differentiation of (40) with respect to R_0 that

$$\frac{\mathrm{d}m^*}{\mathrm{d}R_0} = \left(\frac{a_2 + a_3}{(2m^* - C_1)a_1 a_2 \beta}\right)\left(m^* - \frac{a_0}{a_1}\right). \qquad (45)$$

Notice that $2m^* - C_1 = \pm\sqrt{C_1^2 - 4C_0}$ with $\sqrt{C_1^2 - 4C_0} > 0$ as earlier established. So, for $0 < m^* < \frac{a_0}{a_1}$, from the sign of the computed derivative in (45), m_2^* in (41) is a

decreasing and continuous function of R_0, while m_1^* is an increasing and continuous function of R_0. Thus, for $R_0 < 1$, m_2^* attains its minimum near $R_0 = 1$, which we have shown is greater than $\frac{a_0}{a_1}$ following the recognition of the form of C_1 given by (44). Thus, we have established that for all values of $R_0 < 1$, the positive solution $m_2^* = \frac{1}{2}(C_1 + \sqrt{C_1^2 - 4C_0}) > \frac{a_0}{a_1}$ and must not be seen as a feasible mathematical equilibrium solution for our model whenever the restriction on m^* given by (34) is in place. We next examine the case $R_0 > 1$.

For $R_0 > 1$, $C_1 > 0$ and $C_0 > 0$ and the two solutions of (40), m_1^*, m_2^* of (42), namely $m_{1,2}^* = \frac{1}{2}(C_1 \pm \sqrt{C_1^2 - 4C_0})$, are both real and positive since $C_1^2 - 4C_0 > 0$ so that $\sqrt{C_1^2 - 4C_0} < C_1$, establishing that there are two positive solutions of m^*. However, for these two positive m^* solutions to produce two possible positive steady-state solutions of Eqs. (28)–(32), we require that both solutions be bounded above by $\frac{a_0}{a_1}$ (so that $0 < r_h \le 1$). From (45), we established that m_2^* in (41) is a decreasing and continuous function of R_0, while m_1^* is an increasing and continuous function of R_0. Since $m_1^* \le C_1 < \frac{a_0}{a_1} + \frac{1-\sigma}{\beta}$, following the recognition of the form of C_1 given by (44), it increases from 0 (when $R_0 = 1$) to its maximum which cannot surpass $\frac{a_0}{a_1}$. On the other hand, m_2^* decreases from its value when $R_0 = 1$ to some value $L > \frac{a_0}{a_1}$, an unrealistic value since we expect $0 < m^* < \frac{a_0}{a_1}$. To see that indeed m_2^* is unrealistic, we will regard R_0 as a function of a_1. Notice from (37) that although R_0 depends as well on the parameters a_2, a_3 and σ, R_0 is bounded above by a_1, since $\frac{a_2(1-\sigma)}{a_2+a_3} \in [0, 1]$. So, increases in R_0 for values much larger than unity can be thought of as a corresponding linear increase in a_1. With this in mind, using the definition of D_0, D_1, D_2 from (43) and that of R_0 of Eq. (37), it is quickly verifiable that[2] Eq. (43) reduces to

$$C_1^2 - 4C_0 = \frac{(1-\sigma)^2}{\beta^2} - \frac{2a_0}{a_1}\frac{(1-\sigma)}{\beta} - \frac{2(1-\sigma)}{\beta^2 a_1} + \frac{(\beta a_0 + 1)^2}{\beta^2 a_1^2} + \frac{4a_0 a_3}{\beta a_1^2 a_2}. \quad (46)$$

By using the form of C_1 in Eq. (44), it can be shown that

$$\lim_{a_1 \to \infty} \left(\frac{C_1 + \sqrt{C_1^2 - 4C_0}}{2} - \frac{a_0}{a_1} \right)$$

$$= \lim_{a_1 \to \infty} \left(\frac{1}{2}\left(\frac{1-\sigma}{\beta} - \frac{1}{\beta a_1} \right) + \frac{\sqrt{C_1^2 - 4C_0}}{2} - \frac{1}{2}\frac{a_0}{a_1} \right). \quad (47)$$

$$= \frac{1}{2}\left(\frac{1-\sigma}{\beta} \right) + \frac{1}{2}\sqrt{\frac{(1-\sigma)^2}{\beta^2}} = \frac{1-\sigma}{\beta} > 0.$$

---

[2] $C_1^2 - 4C_0 = \left(D_2 R_0^2 - D_2 D_1 R_0 + D_2 D_0 \right)$, where $D_2 R_0^2 = \frac{(1-\sigma)^2}{\beta^2}$, $D_2 D_1 R_0 = \frac{2a_0}{a_1}\frac{(1-\sigma)}{\beta} + \frac{2(1-\sigma)}{\beta^2 a_1}$ and $D_2 D_0 = \frac{a_2^2(\beta a_0+1)^2 + 4\beta a_0 a_2 a_3}{\beta^2 a_1^2 a_2^2}$.

Since the just computed limit is a positive quantity, we have thus shown that there exists $N_{a_1} > 0$ such that $(m_2^* - \frac{a_0}{a_1})$ will have the same sign as $\frac{1-\sigma}{\beta}$ whenever $a_1 > N_{a_1}$. That is there exists $N_{a_1} > 0$ such that $0 < m_2^* - \frac{a_0}{a_1} < 2\frac{1-\sigma}{\beta}$ whenever $a_1 > N_{a_1}$. Thus, m_2^* is bounded below by $\frac{a_0}{a_1}$ for large values of a_1 and hence for large values of R_0. We therefore conclude that system (28)–(32) under study has a unique parasitized equilibrium solution where $m^* \neq 0$ given by $m^* = m_1^*$ as defined in (41) which is positive and bounded above by $\frac{a_0}{a_1}$ for $R_0 > 1$ or $a_1 > \frac{a_2+a_3}{a_2(1-\sigma)}$ and coexists with the trivial and parasite-free steady states. This completes the proof of the theorem. $\qquad \square$

Remark 1 (i) The foregoing discussion shows that the steady-state solutions of the system (28)–(32) are uniquely determined and depend on R_0 as well as on the size of the quantity $\frac{a_0}{a_1}$, as provided by the delimitation set by (34). That is, realistic nonzero solutions are those for which m^* and r_h^* remain bounded and are given by $m^* = m_1^*$ and exists only when $R_0 > 1$ or $a_1 > \frac{a_2+a_3}{a_2(1-\sigma)}$.

(ii) From (46), given the form of C_1 in (44), we easily establish that

$$\lim_{a_1 \to \infty} \left(\frac{C_1 - \sqrt{C_1^2 - 4C_0}}{2} - \frac{a_0}{a_1} \right) = \frac{1}{2}\left(\frac{1-\sigma}{\beta}\right) - \frac{1}{2}\sqrt{\frac{(1-\sigma)^2}{\beta^2}} = 0, \quad (48)$$

showing that m_1^* asymptotically approach its upper bound $\frac{a_0}{a_1}$.

(iii) Implicit differentiation of Eq. (40) with respect to R_0 yields,

$$\frac{\mathrm{d}^2 C_0}{\mathrm{d}R_0^2} - C_1 \frac{\mathrm{d}^2 m^*}{\mathrm{d}R_0^2} - \frac{\mathrm{d}C_1}{\mathrm{d}R_0}\frac{\mathrm{d}m^*}{\mathrm{d}R_0} - \frac{\mathrm{d}m^*}{\mathrm{d}R_0}\frac{\mathrm{d}C_1}{\mathrm{d}R_0}$$
$$- m^* \frac{\mathrm{d}^2 C_1}{\mathrm{d}R_0^2} + 2\frac{\mathrm{d}m^*}{\mathrm{d}R_0}\frac{\mathrm{d}m^*}{\mathrm{d}R_0} + 2m^* \frac{\mathrm{d}^2 m^*}{\mathrm{d}R_0^2} = 0,$$

for any m^*. From (42), $\frac{\mathrm{d}C_0}{\mathrm{d}R_0} = \frac{a_0(a_2+a_3)}{\beta a_1^2 a_2} \Rightarrow \frac{\mathrm{d}^2 C_0}{\mathrm{d}R_0^2} = 0$, $\frac{\mathrm{d}C_1}{\mathrm{d}R_0} = \frac{a_2+a_3}{\beta a_1 a_2} \Rightarrow \frac{\mathrm{d}^2 C_1}{\mathrm{d}R_0^2} = 0$, which when substituted into the last equation yields

$$(2m^* - C_1)\frac{\mathrm{d}^2 m^*}{\mathrm{d}R_0^2} - 2\frac{\mathrm{d}m^*}{\mathrm{d}R_0}\left(\frac{\mathrm{d}C_1}{\mathrm{d}R_0} - \frac{\mathrm{d}m^*}{\mathrm{d}R_0}\right) = 0,$$

upon simplification. Furthermore, substituting Eq. (45) into the last expression and simplifying further leads to

$$\frac{\mathrm{d}^2 m_1^*}{\mathrm{d}R_0^2} = \frac{a_2+a_3}{\beta a_1 a_2}\frac{2\frac{\mathrm{d}m_1^*}{\mathrm{d}R_0}}{(2m_1^* - C_1)}\left(1 - \frac{m_1^* - \frac{a_0}{a_1}}{2m_1^* - C_1}\right)$$
$$= -2\left(\frac{a_2+a_3}{\beta a_1 a_2}\right)^2 \left(\frac{\left(m_1^* - \frac{a_0}{a_1}\right)\left(m_2^* - \frac{a_0}{a_1}\right)}{(2m_1^* - C_1)^3}\right),$$

when $m^* = m_1^*$. But, $m_1^* < \frac{a_0}{a_1}$, $m_2^* > \frac{a_0}{a_1}$ and $\frac{dm_1^*}{dR_0} > 0$ which implies that $\frac{d^2 m_1^*}{dR_0^2} < 0$. Thus, m_1^* increases at a decreasing rate, asymptotically approaching its upper bound $\frac{a_0}{a_1}$.

Remark 2 R_0 determined and defined in (37) is the unique threshold parameter for the system when the conditions of the theorem are satisfied. Its value is uniquely determined by the parameters a_2, a_3 and σ, and represents an invasion criterion as we introduce infection in the system. It is directly proportional to a_1, with proportionality constant $\frac{a_2(1-\sigma)}{a_2+a_3} < 1$; thus, it is bounded above by a_1, i.e. $R_0 \leq a_1$. Therefore, R_0 increases with increasing a_1, and so we regard an increase in R_0 from one as an increase in a_1, since R_0 can never grow beyond a_1. However, a decrease in R_0 towards zero is not as simple, since the path $R_0 \to 0$ could be along $a_2 \to 0$, or $a_3 \to \infty$ or along the path $\sigma \to 1$.

Remark 3 Notice that in non-dimensional form, the parasitemia reproduction number defined in Eq. (37) has the same expression for both choices of $g(r_h)$, either $g(r_h) = 1 - r_h$ or $g(r_h) = r_h(1 - r_h)$. However, in the original parameters, that is not the case. Using the original parameters to rewrite this reproduction number, we see that the parasitemia reproduction number is:

(i) for $g(r_h) = 1 - r_h$,
$$\mathcal{R}_0 = \frac{a_1 a_2 (1 - \sigma)}{a_3 + a_2} = \frac{\beta_1 r \gamma_p \Theta (1 - \sigma)}{(\beta_2 \Theta + \mu_h \mu_m)(\gamma_p + \mu_p)}, \tag{49}$$
(ii) for $g(r_h) = r_h(1 - r_h)$,
$$\mathcal{R}_0 = \frac{a_1 a_2 (1 - \sigma)}{a_3 + a_2} = \frac{\beta_1 r \gamma_p (\Lambda - \mu_h)(1 - \sigma)}{(\beta_2 (\Lambda - \mu_h) + \widetilde{\mu}_h \mu_m)(\gamma_p + \mu_p)}. \tag{50}$$

We now graphically illustrate the results of Theorem 4 when $g(r_h) = r_h(1 - r_h)$, i.e. item 2 of the theorem. We will also describe the biological implications associated with the results with regard to the onset and existence of a parasitized steady state. The proof of the case when $g(r_h) = 1 - r_h$ was straight forward and does not warrant attention at this point.

Figures 2 and 3 show the behaviours of the steady-state solution m_1^* and m_2^* (see Eqs. (41) and (40)) as well as the threshold parameter R_0 and the bound $\frac{a_0}{a_1}$, in relation to changes in the size of a_1, for different choices of parameters that are related to these functions, when the recruitment function is $g(r_h) = r_h(1 - r_h)$. In both figures, the m_1^* curve is always below the $\frac{a_0}{a_1}$ curve, while the m_2^* curve is always above. Moreover, the point of intersection between the linear R_0 curve and the horizontal green line occurs at $R_0 = 1$. This is also the point at which the steady state m_1^* is zero. These results corroborate the proof of item 2 in Theorem 4 as we now describe. If $R_0 \leq 1$ (i.e. the R_0 curve is below the horizontal green line or intersects it), there is a unique real positive merozoite steady-state solution for m^*, which is m_2^* (the red curve), but it does not yield a real positive parasitized equilibrium solution within the bounds of Eq. (34). For this case, the only steady-state solution of system (28)–(32) will be the parasite-free steady state, $\mathbf{x}_{pf}$. At $R_0 = 1$ (the intersection point), m_1^* is zero, with the emergence of
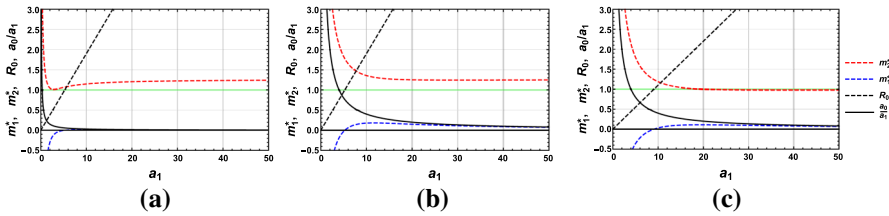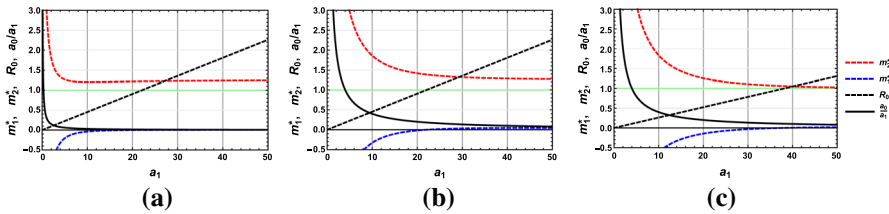
Fig. 2 Plots of the steady-state solutions, m_1^* (the blue dashed curve) and m_2^* (the red dashed curve), and of R_0 (the black dotted linear curve) and the bound $\frac{a_0}{a_1}$ (the solid black decaying curve), plotted against a_1, showing their profiles as well as limiting behaviours for large values of a_1. For all the graphs, **a**, **b** and **c**, feasible parameter values are chosen with $a_2 = 0.5$ and $a_3 = 2$, while allowing for β, σ and a_0 to vary for values within their range as given in Eq. (33). **a** Plots for $\beta = 0.75$, $\sigma = 0.05$, $a_0 = 0.3$ and $a_2 = 0.5$. **b** Plots for $\beta = 0.75$, $\sigma = 0.05$, $a_0 = 4$ and $a_2 = 0.5$. **c** Plots for $\beta = 0.55$, $\sigma = 0.45$, $a_0 = 4$ and $a_2 = 0.5$ (Color figure online)

Fig. 3 Plots of the steady-state solutions, m_1^* (the blue dashed curve) and m_2^* (the red dashed curve), and of R_0 (the black dotted linear curve) and the bound $\frac{a_0}{a_1}$ (the solid black decaying curve), plotted against a_1, showing their profiles as well as limiting behaviours for large values of a_1. For all the graphs, **a**, **b** and **c**, feasible parameter values are chosen with, feasible parameter values are chosen with $a_2 = 0.1$, less than the value used in Fig. 2 while $a_3 = 2$ remains unchanged; meanwhile, we allow β, σ and a_0 to vary for values within their range as given in Eq. (33). **a** Plots for $\beta = 0.75$, $\sigma = 0.05$, $a_0 = 0.3$ and $a_2 = 0.1$. **b** Plots for $\beta = 0.75$, $\sigma = 0.05$, $a_0 = 4$ and $a_2 = 0.1$. **c** Plots for $\beta = 0.55$, $\sigma = 0.45$, $a_0 = 4$ and $a_2 = 0.1$ (Color figure online)

a positive parasitized steady state for m_1^*, bounded above by $\frac{a_0}{a_1}$ as R_0 increases beyond 1. That is, for $R_0 > 1$, there are two real positive merozoite steady-state solutions for m^*, (here both m_1^* and m_2^* are positive) but only one (m_1^*) leads to a unique real positive parasitized equilibrium solution within $(0, \frac{a_0}{a_1})$, the bounds as defined in Eq. (34). The other, m_2^*, is bounded below by the $\frac{a_0}{a_1}$ curve and falls outside the bounds of Eq. (34). We note that we have graphically shown scenarios where the m_1^* curve goes negative in order to showcase the instance when a non-trivial m_1^* solution emerges (which can be thought of as the emergence of parasitemia). Biologically, however, the negative m_1^* values are unrealistic. It basically implies there is not a realistic m_1^* solution and the only steady state in this case is the parasite-free steady state, $\mathbf{x}_{pf}$.

We next discuss the role parameter changes have in Figs. 2 and 3. To do so, we first convert to original variables. In terms of the original variables, $a_1 = \frac{\beta_1 r \gamma_p}{\beta_2(\mu_p + \gamma_p)} < \frac{\beta_1}{\beta_2} r$, $\beta = \frac{\beta_3}{\beta_2} \leq 1$ and $a_3 = \frac{\mu_m}{\mu_p + \gamma_p} > 1$, all positive. For $g(r_h) = r_h(1 - r_h)$, $a_0 = \frac{\Lambda - \mu_h}{\mu_p + \gamma_p}$ and $a_2 = \frac{\beta_2(\Lambda - \mu_h)}{\mu_h(\mu_p + \gamma_p)}$, both positive, and with R_0 as defined in Eqs. (37) and (50). By rewriting $a_1 = \frac{\beta_1 r \gamma_p a_0}{\beta_2(\Lambda - \mu_h)}$, $a_2 = \frac{\beta_2 a_0}{\tilde{\mu}_h}$ and also R_0 (see Eq. (37)) in terms of a_0, we see that there are parameter regimes for which we can vary a_0 while allowing both

a_1 and a_2, as well as R_0 to take a desired form, by adjusting the other parameters not associated with a_0. By comparing graphs (a) and (b) of Figs. 2 and 3, we see that for a fixed β and σ, increasing the size of a_0 with the other parameters chosen such that a_2 is fixed as shown in the figures, results in a larger a_1 value. This makes sense in that an increase in a_0 as described above will likely be as a result of an increase in the growth term $\Lambda - \mu_h$, of the recruitment function of the healthy red blood cells. A larger $\Lambda - \mu_h$ value implies more HRBCs will be available for potential parasitization. This increase in a_0, however, does not yield a large noticeable increase in the size of R_0 because in Eq. (50), the term $\widetilde{\mu}_h \mu_m$, which is fixed, dominates in the expression $\beta_2(\Lambda - \mu_h) + \widetilde{\mu}_h \mu_m$, since the death rate of free floating merozoites has a dominant effect (see Table 3 and the discussion in Sect. 4.1).

Next, if we select parameters that allow for a lower a_2 value, with all other expressions remaining unchanged, we see that the rates of decay of m_2^* and the rate of growth of m_1^*, both with respect to changes in a_1, decrease (compare graphs (a) and (b) of Fig. 2 to graphs (a) and (b) of Fig. 3, respectively). A decrease in a_2 as described is likely the result of an increase in the additional death rate, $\widetilde{\mu}_h$, of healthy red blood cells. Here, however, the impact of reducing a_2 as a result of a likely increase in $\widetilde{\mu}_h$, is noticeable on the size of R_0. This is reasonable because from Eq. (50), an increase $\widetilde{\mu}_h$ increases the dominant term $\widetilde{\mu}_h \mu_m$, and as a result produces a larger effect on slowing the increase of R_0 to values bigger than 1. Hence, a larger a_1 value, which will likely be due to a larger β_1 (contact rate between HRBCs and free floating merozoites) value or a larger r (number of parasites released per bursting IRBCs) value, will be needed for parasitemia to commence.

The factor $\sigma \in [0, 1]$, which is the proportion of infected red blood cells that continue towards the path of gametocytogenesis, does not directly influence the size of a_0, a_1 or a_2 but has a strong influence on the size of the parasitized steady states as well as the threshold parameter R_0 (compare graphs (b) to (c) for both Figs. 2 and 3). In particular, for all other parameters held fixed, as σ increases towards 1 (meaning more parasitized red blood cells continue the path towards gametocytogenesis and hence an expectation of a higher gametocyte load), $R_0 \to 0$. Thus, a larger a_1 value will be required for the onset of parasitemia. The implication here is that, for larger values of σ, there will be fewer parasitized red blood cells continuing the cyclical path towards producing more merozoites. Upon bursting then, fewer merozoites will be available to infect HRBCs, unless the number of merozoites produced per bursting red blood cell is large enough (equivalent to a larger r and hence a larger a_1 value). This, nonetheless, does not imply the individual is less infectious. On the flip side, that may not be the case, especially if there is no interference with the developmental and maturation process of early-state gametocytes. If we assume a positive correlation between the size of the gametocyte load and infectiousness to mosquitoes as assumed in Teboh-Ewungkem et al. (2010) and further discussed in Teboh-Ewungkem and Yuster (2010), then this scenario depicts a more infectious individual even though the merozoite load may not be as high.

A similar discussion can be given for the parameter β. In conclusion, an increase in a_1 leads to a linear increase in R_0, while $m_1^* \to \frac{a_0}{a_1}$ from below and $m_2^* \to M > \frac{a_0}{a_1}$ from above. From Eq. (47), the $\lim\limits_{a_1 \to \infty} \left(m_2^* - \frac{a_0}{a_1} \right) = \frac{1-\sigma}{\beta} > 0$, which gives a measure

of the limiting distance between the $\frac{a_0}{a_1}$ curve and the m_2^* curve in Figs. 2 and 3. This distance will be large for small β values as well as for small σ values (i.e. σ values closer to zero), as highlighted in the figures. Smaller sigma values also correspond to larger values of R_0 for all other parameters held fixed. On the other hand, from Eq. (48), the $\lim_{a_1 \to \infty} \left(m_1^* - \frac{a_0}{a_1} \right) = 0$ which indicates that for fixed parameters, the size of m_1^* is bounded above by $\frac{a_0}{a_1}$, which in terms of the original variables gives $\frac{a_0}{a_1} = \frac{\beta_2(\Lambda - \mu_h)}{\beta_1 r \gamma_p}$. Thus, for large a_1 values, corresponding more to either a large r value (more merozoites released per bursting red blood cells), or large β_1 value (higher contact rate between free merozoites and HRBCs) and small β_2 (less free floating merozoites being absorbed by IRBCs), the bound $\frac{a_0}{a_1}$ will be small, if $\Lambda - \mu_h$ is relatively small, corresponding to a small a_0 value (see graph (a) of Figs. 2 and 3). That is, the merozoite load would not be expected to be high. The rational is that although the scenarios described (large r, large β_1 and small β_2) correspond to situations where HRBCs should have higher opportunities to interact and be infected by free floating parasites, the HRBC load is not high enough because of the small recruitment term $\Lambda - \mu_h$ leading to the overall low small bound. On the other hand, if $\Lambda - \mu_h$ is larger, corresponding to a large a_0 value (see graphs (b) and (c) of Figs. 2 and 3), we will expect a higher bound for smaller a_1, with the bound decreasing with increasing a_1, for a_0 fixed. Here, since $\Lambda - \mu_h$ is large, the density of HRBCs would be expected to be higher contributing to the increase in the size of the bound, especially for smaller a_1.

4.2.2 Stability of Steady States

The next result concerns the local stability of the identified steady-state solutions.

Theorem 5 *Let the condition of Theorem 4 continue to hold, and let R_0 be as defined in (37). Then,*

1. *The trivial steady state $\boldsymbol{x}_0 = (0, 0, 0, 0, 0)$, which always exist for $g(r_h) = r_h(1 - r_h)$, is locally unstable for all values of R_0.*
2. *The parasite-free state $\boldsymbol{x}_{pf} = (1, 0, 0, 0, 0)$, which always exists for both forms of $g(r_h)$, is locally and asymptotically stable whenever $R_0 \le 1$ and unstable otherwise.*
3. *When $g(r_h) = 1 - r_h$, the non-trivial parasitized steady state, which only exists and is uniquely determined for all $R_0 > 1$ is locally and asymptotically stable.*
4. *When $g(r_h) = r_h(1 - r_h)$, the non-trivial parasitized steady state, which in this case only exists and is uniquely determined for $R_0 > 1$ with $m^* < \frac{a_0}{a_1}$, is locally and asymptotically stable to small perturbations.*

Proof Let $\boldsymbol{x}_0^* = (0, 0, 0, 0, 0)$ be the trivial steady state, $\boldsymbol{x}_{pf}^* = (1, 0, 0, 0, 0)$ be the parasite-free state and $\boldsymbol{x}_e^* = (r_h^*, r_p^*, m^*, g_e^*, g_l^*)$ be the non-trivial parasitized steady state when $R_0 > 1$ and the respective values are given by Theorem 4. Then, the stability of any steady state $\boldsymbol{x}^* = (r_h^*, r_p^*, m^*, g_e^*, g_l^*)$ is determined by the eigenvalues of the

Jacobian matrix at the steady state x^*. Let $J(x^*)$ be the Jacobian matrix at the steady state x^*. Here,

$$J(x^*) = \begin{pmatrix} a_0 g'(r_h^*) - m^* a_1 & 0 & -r_h^* a_1 & 0 & 0 \\ m^* a_1 & -1 & r_h^* a_1 & 0 & 0 \\ -m^* a_2 & (-m^*\beta - \sigma + 1)a_2 & -(r_h^* + r_p^*\beta)a_2 - a_3 & 0 & 0 \\ 0 & \sigma a_4 & 0 & -a_4 & 0 \\ 0 & 0 & 0 & a_5 & -a_5 \end{pmatrix}. \tag{51}$$

Now, if λ is an eigenvalue of $J(x^*)$, then λ satisfies the equation

$$|\lambda I - J(x^*)| = (\lambda + a_5)(\lambda + a_4)P_3(\lambda, x^*) = 0, \tag{52}$$

where $P_3(\lambda, x^*)$ is the third-degree polynomial

$$P_3(\lambda, x^*) = \begin{vmatrix} \lambda - a_0 g'(r_h^*) + m^* a_1 & 0 & r_h^* a_1 \\ -m^* a_1 & \lambda + 1 & -r_h^* a_1 \\ m^* a_2 & (m^*\beta + \sigma - 1)a_2 & \lambda + (r_h^* + r_p^*\beta)a_2 + a_3 \end{vmatrix}.$$

Expansion of P_3 defined in (52) yields

$$P_3(\lambda, x^*) = \lambda^3 + P(x^*)\lambda^2 + Q(x^*)\lambda + R(x^*), \tag{53}$$

where

$$P(x^*) = -a_0 g'(r_h^*) + a_1 m^* + a_2(r_h^* + \beta r_p^*) + a_3 + 1$$

$$Q(x^*) = -a_0 g'(r_h^*)\left(a_2(r_h^* + \beta r_p^*) + a_3 + 1\right)$$
$$+ a_1\left(a_2(r_h^*(\beta m^* + \sigma - 1) + \beta m^* r_p^*) + a_3 m^* + m^*\right) + a_2 r_h^* + a_2 \beta r_p^* + a_3$$

$$R(x^*) = a_1\left(a_2\left(\beta m^* r_p^* - a_0 r_h^* g'(r_h^*)(\beta m^* + \sigma - 1)\right) + a_3 m^*\right)$$
$$- a_0 g'(r_h^*)\left(a_2(r_h^* + \beta r_p^*) + a_3\right).$$

We now consider several possibilities. When $g(r_h) = r_h(1 - r_h)$, then $g'(r_h) = 1 - 2r_h$ and at the trivial steady state $x_0 = (0, 0, 0, 0, 0)$, which always exist whenever $g(r_h) = r_h(1 - r_h)$, the coefficients of the cubic (53) take the form

$$P(x_0) = -a_0 + a_3 + 1, \quad Q(x_0) = a_3 - a_0(a_3 + 1), \quad R(x_0) = -a_0 a_3,$$

so that (53) factorizes into $P_3(\lambda, x_0^*) = (\lambda - a_0)(\lambda + a_3)(\lambda + 1)$ indicating the presence of exponentially growing perturbations with positive eigenvalue a_0. Hence, that steady-state solution is unstable to small perturbations. This establishes part one of the theorem.

Next, we establish the stability of the parasite-free steady state $x_{pf} = (1, 0, 0, 0, 0)$. Notice that for both forms of $g(r_h)$ in (26), $g'(1) = -1$. Hence, the stability matrices

at this steady state, which always exist for both forms of $g(r_h)$, coincide, and the coefficients of the cubic (53) take the form

$$P(x_{pf}^*) = a_0 + a_2 + a_3 + 1, \quad Q(x_{pf}^*) = a_0 (a_2 + a_3 + 1) - (a_2 + a_3) (R_0 - 1),$$
$$R(x_{pf}^*) = -a_0 (a_2 + a_3) (R_0 - 1)$$

so that (53) factorizes into $P_3(\lambda, x_{pf}^*) = (\lambda + a_0)(\lambda^2 + T\lambda + S)$ where $T = a_2 + a_3 + 1$ and $S = (a_2 + a_3)(1 - R_0)$. It then becomes immediately clear that whenever $R_0 < 1$, there are no solutions with positive real part that will signify exponentially growing perturbations in the linear regime, and the parasite-free steady state is always locally and asymptotically stable whenever $R_0 < 1$. On the other hand, if $R_0 > 1$ there is at least one real and positive solution of (52) signifying exponentially growing perturbations in the linear regime and the merozoite-free state is unstable. This establishes the proof or part two of the theorem.

To proof part three of the theorem, for the case where $g(r_h) = 1 - r_h$, the equilibrium point x_e, where all cell types are positive, is uniquely determined and the coefficients of the polynomial (53) take the form

$$P(x_e) = \frac{p_2(R_0 - 1)^2 + p_1(R_0 - 1) + p_0}{p_3 + p_4(R_0 - 1)},$$
$$Q(x_e) = \frac{q_2(R_0 - 1)^2 + q_1(R_0 - 1) + q_0}{q_3 + q_4(R_0 - 1)},$$
$$R(x_e) = r_0 (R_0 - 1), \tag{54}$$

where

$$p_1 = (a_2 + a_3) (a_0 a_2 \beta + a_3) (a_0 (a_2 \beta + 2) + a_3 + 1), \quad r_0 = a_0 (a_2 + a_3)$$
$$p_0 = (a_0 + a_2 + a_3 + 1) (a_0 a_2 \beta + a_3)^2, \quad p_2 = a_0 (a_2 + a_3)^2$$
$$p_4 = (a_2 + a_3) (a_0 a_2 \beta + a_3), \quad p_3 = (a_0 a_2 \beta + a_3)^2$$
$$q_2 = a_0 (a_2 + a_3)^2 (a_0 a_2 \beta + a_3 + 1), \quad q_3 = (a_0 a_2 \beta + a_3)^2$$
$$q_1 = a_0 (a_2 + a_3) (a_0 a_2 \beta + a_3) ((a_0 + 1) a_2 \beta + 2 (a_3 + 1)),$$
$$q_0 = a_0 (a_2 + a_3 + 1) (a_0 a_2 \beta + a_3)^2, \quad q_4 = (a_2 + a_3) (a_0 a_2 \beta + a_3)$$

Clearly, P, Q, R in (54) are all positive when $R_0 > 1$. Thus, there is no sign change in the sequence of coefficients for the characteristic polynomial indicating the absence of positive real roots of (53). To be assured that equilibrium is indeed locally and asymptotically stable, we use the Routh–Hurwitz stability criteria and verify that $P(x_e)Q(x_e) - R(x_e) > 0$. On expanding this quantity out, we find that it can be written in the form

$$d_4(R_0 - 1)^4 + d_3(R_0 - 1)^3 + d_2(R_0 - 1)^2 + d_1(R_0 - 1)$$
$$+ d_0 > 0 \text{ whenever } R_0 > 1. \tag{55}$$

Here,

$$d_4 = p_2 q_2, \ d_3 = p_2 q_1 + p_1 q_2 - r_0 p_4 q_4, \ d_2 = P_2 q_0 + p_1 q_1 + p_0 q_2 - r_0 (p_3 q_4 + p_4 q_3)$$
$$d_1 = p_1 q_0 + p_0 q_1 - r_0 p_3 q_3, \ d_0 = p_0 q_0,$$

which on simplification yields,

$$d_4 = a_0^2 (a_2 + a_3)^4 (a_0 a_2 \beta + a_3 + 1)$$
$$d_3 = a_0 (a_2 + a_3)^3 (a_0 a_2 \beta + a_3) \left(a_2 a_0^2 \beta (a_2 \beta + 3) \right.$$
$$\left. + 2 (a_3 + 1) a_0 (a_2 \beta + 2) + a_3^2 + a_3 + 1 \right)$$
$$d_2 = a_0 (a_2 + a_3)^2 (a_0 a_2 \beta + a_3)^2 (A_1 + A_2)$$
$$d_1 = a_0 (a_2 + a_3) (a_0 a_2 \beta + a_3)^3 (A_3 + A_4)$$

with

$$A_1 = a_2 a_0^2 \beta (a_2 \beta + 3) + a_2 (a_3 + 1) (\beta + 1) + a_3 (3a_3 + 4) + 3,$$
$$A_2 = a_0 (a_2 (a_2 (\beta + 1) \beta + 4a_3 \beta + 4\beta + 1) + 6 (a_3 + 1))$$
$$A_3 = a_2 a_0^2 \beta + a_2^2 \beta + a_2 (a_3 + 1) (\beta + 3) + a_3 (3a_3 + 5) + 3$$
$$A_4 = 2a_0 (a_2 ((a_2 + a_3) \beta + \beta + 1) + 2 (a_3 + 1)).$$

This clearly demonstrates that when the non-trivial steady state is uniquely determined, it is locally and asymptotically stable to small perturbations. This completes the proof of part three of the theorem.

For the case where $g(r_h) = r_h(1 - r_h)$, as shown by the proof of Theorem 4, the steady-state solution where all cell types are nonzero is x_e, and now exist only under certain restrictions and so its stability properties are no longer as straight forward. We start by noting that for the steady state $r_h^*(m^*)$ defined by (39) to be realistic in the context of the scaling in this manuscript, the solution m^* delimited by the bounds (34) must satisfy the Eq. (40) and when the solution $m_1^* = \frac{1}{2}(C_1 - \sqrt{C_1^2 - 4C_0})$ is substituted into the polynomial (53), we obtain expressions which are essentially very complicated to be useful, given the restrictions needed in each case. Nevertheless, we can say something about the stability of the steady state in this case by noting the following: At the equilibrium point, using the relations (39) along side the original equations for the steady states, we have the following relationships between the steady states: $a_1 m^* = a_0 (1 - r_h^*), a_3 + a_2 (r_h + \beta r_p) = a_1 a_2 (1 - \sigma) r_h = (a_2 + a_3) R_0 r_h^*$ so that we can use these together with the fact that when $g(r_h) = r_h (1 - r_h), a_0 g'(r_h^*) - a_1 m^* = -a_0 r_h^*$, in the coefficients of characteristic polynomial to have

$$P(x_e) = 1 + p_1 a_0 r_h^*, \ Q(x_e) = a_0 r_h^* (q_0 + q_1 a_0 r_h^*),$$
$$R(x_e) = a_0^2 r_h^* (1 - r_h^*)(r_0 + r_1 (a_0 r_h^*)) \tag{56}$$

where

$$p_1 = \left(\frac{a_0 + (a_2 + a_3)R_0}{a_0}\right), \quad q_0 = 1 - a_2(1 - \beta), \quad q_1 = \frac{a_2(1 - \beta) + (a_2 + a_3)R_0}{a_0}$$
$$r_0 = \frac{a_2(R_0 - (1 + a_0\beta)) + a_3 R_0}{a_0}, \quad r_1 = \frac{2\beta a_2}{a_0}$$

(57)

Notice that $p_1 > 0$ and so P is always positive. Furthermore, Q and R will also be positive whenever $q_0 > 0$, $r_0 > 0$ and $r_h^* < 1$. Now, positivity of q_0 is guaranteed whenever $a_2 < \frac{1}{1-\beta}$ while the positivity of r_0 is guaranteed if $R_0 > \frac{a_2(1 + a_0\beta)}{a_2 + a_3}$. When these conditions, which are sufficient but may not be necessary, are satisfied, we are sure that there are no positive real roots for the polynomial (53) which will signify exponentially growing perturbations in linear regime. Again to be certain that the steady state will indeed be stable when these conditions hold we apply the Routh–Hurwitz condition to have

$$P(\boldsymbol{x}_e)Q(\boldsymbol{x}_e) - R(\boldsymbol{x}_e) = a_0 r_h^* \left(a_0^2 c_2 (r_h^*)^2 + c_1 a_0 r_h^* + c_0\right),$$

where from (56) and (57),

$$c_2 = p_1 q_1 + r_1, \quad c_1 = q_1 + p_1 q_0 + r_0 - a_0 r_1, \quad c_0 = q_0 - a_0 r_0.$$

If the coefficients c_2, c_1 and c_0 are also positive, then we are certain that the steady state is locally stable to small perturbations. Now, when the conditions $a_2 < \frac{1}{1-\beta}$ and $R_0 > \frac{a_2(1 + a_0\beta)}{a_2 + a_3}$ continue to hold, we quickly establish that the positivity of c_1 is guaranteed if $a_3 > \frac{2a_2 a_0 \beta}{1 + a_0\beta}$ and that $c_0 = 1 + (a_0 + 1) a_2\beta - (a_2 + a_3) R_0$ is positive whenever $R_0 < \frac{1 + a_2(1 + a_0\beta)}{a_2 + a_3}$. This leads to the establishment of a stability window delimited by the inequalities

$$R_0 > 1, \quad \frac{a_2(1 + a_0\beta)}{a_2 + a_3} < R_0 < \frac{1 + a_2(1 + a_0\beta)}{a_2 + a_3}, \quad a_2 < \frac{1}{1 - \beta}, \quad a_3 > \frac{2a_2 a_0 \beta}{1 + a_0\beta},$$

which are sufficient, but may not be necessary, for the stability of the steady state in the logistic case. This completes the proof of the theorem. □

We have thus established that the stability properties for all the steady states of the system, under the restricted condition of immunity suppression, can be and have been characterized. The analysis shows that any oscillatory solutions must be damped oscillations in time, for all types of birth rate functions studied. We shall illustrate these results numerically, in Sect. 5.

The next result concerns the global stability of the identified parasite-free steady-state solution, $\boldsymbol{x}_{pf}$, when $R_0 \leq 1$.

Theorem 6 *For the immune-suppressed system, Eqs. (28)–(32), the parasite-free steady state $\boldsymbol{x}_{pf} = (1, 0, 0, 0, 0)$ is globally asymptotically stable for both forms of $g(r_h)$ when $R_0 \leq 1$. That is, the parasite-free steady state attracts all solution of the system in $\mathbb{R}_+^5$ for $R_0 \leq 1$.*

Proof (i) $g(r_h) = 1 - r_h$. The proof is immediate since for this form of $g(r_h)$, $\boldsymbol{x}_{pf} = (1, 0, 0, 0, 0)$ is the only steady state when $R_0 \leq 1$.

(ii) $g(r_h) = r_h(1 - r_h)$. Let us define the compact region

$$D_0 = \left\{ (r_h, r_p, m, g_e, g_l) \in \mathbb{R}^5 : \varepsilon \leq r_h \leq 1, 0 \leq r_p \leq r_p^\infty, \right.$$
$$\left. 0 \leq m \leq m^\infty, 0 \leq g_e \leq g_e^\infty, 0 \leq g_l \leq g_l^\infty \right\},$$

where $0 < \varepsilon \ll 1$ and $r_p^\infty, m^\infty, g_e^\infty, g_l^\infty$ are the respective standardized upper bounds of the associated variables obtained from the upper bounds $R_p^\infty, M^\infty, G_e^\infty, G_l^\infty$ as proved in Theorem 2 in Sect. 2.3, under the assumptions of the immune-suppressed model. Then, system (28)–(32) has a unique steady state in $\mathcal{D}_0$ when $R_0 \leq 1$, and it is $\boldsymbol{x}_{pf}$. Next, define the Lyapunov function

$$V : (r_h, r_p, m, g_e, g_l) \in (0, 1] \times \mathbb{R}^4_+ \to \mathbb{R},$$

where

$$V(r_h, r_p, m, g_e, g_l) = A(r_h - 1 - \ln r_h) + Br_p + Cm + Dg_e + Eg_l. \quad (58)$$

The coefficients A, B, C, D and E are positive constants to be chosen such that the time derivative of V is negative definite (i.e. $V' < 0$) for all $\mathbf{x} \neq \mathbf{x}_{pf}$, whenever $R_0 \leq 1$. In particular, if we choose C to be any constant greater than 1, and define

$$D = (C - 1)(a_3 + a_2)\frac{(1 - R_0)}{a_1 a_4 \sigma}, \quad E = D\frac{a_4}{a_5}, \quad A = (C - 1)\frac{a_3}{a_1};$$
$$B = Ca_2(1 - \sigma) + Da_4\sigma, \quad (59)$$

then $A > 0$ and B, C, D and E are all non-negative whenever $R_0 \leq 1$. Moreover, from Eq. (59), it is easily seen that

$$Da_4 - Ea_5 = 0, \quad Ca_2(1 - \sigma) - B + Da_4\sigma = 0 \text{ and } Aa_1 - Ca_3 = -a_3,$$

and it can be verified that

$$-Aa_1 + Ba_1 - Ca_2 = a_1a_2(1 - \sigma) - a_2 = (a_3 + a_2)R_0 - a_2.$$

Additionally, since $r_h < 1 \Rightarrow -m < -mr_h$ and we have that

$$V' = A\left(1 - \frac{1}{r_h}\right)r_h' + Br_p' + Cm' + Dg_e' + Eg_l'$$
$$= A\left(1 - \frac{1}{r_h}\right)\left[a_0r_h(1 - r_h) - a_1r_hm\right] + B\left[a_1r_hm - r_p\right]$$
$$\quad + C[a_2(1 - \sigma)r_p - a_2r_hm - a_2\beta r_pm - a_3m] + Da_4[\sigma r_p - g_e] + Ea_5[g_e - g_l]$$
$$= -Aa_0(1 - r_h)^2 + \left[Aa_1(1 - r_h)m + Ba_1r_hm\right] - Br_p + Ca_2(1 - \sigma)r_p$$
$$\quad - Ca_2r_hm - Ca_2\beta r_pm - Ca_3m + Da_4\sigma r_p - Da_4g_e + Ea_5g_e - Ea_5g_l$$

Table 4 Stability properties of the steady states $x_0 = (0, 0, 0, 0, 0)$, $x_{pf} = (1, 0, 0, 0, 0)$ and $x_e = (r_h^*, r_p^*, m_1^*, g_e^*, g_l^*)$ of system (28)–(32) for the two forms of the recruitment function $g(r_h)$ as prescribed by Theorem 4

$g(r_h)$	Type of steady state	Existence	Stability	Restriction
$1 - r_h$	Trivial, x_0	DNE	–	–
	Parasite-free (PFSS), x_{pf}	Always exists	GAS	$0 \le R_0 \le 1$
		Always exists	Unstable	$R_0 > 1$
	Non-trivial, x_e (ESS)	Exists	LAS	$R_0 > 1$
$r_h(1 - r_h)$	Trivial, x_0	Always exists	Unstable	$R_0 \ge 0$
	Parasite-free (PFSS), x_{pf}	Always exists	GAS	$0 \le R_0 \le 1$
		Always exists	Unstable	$R_0 > 1$
	Non-trivial (ESS), x_e	Exists	LAS	$R_0 > 1, m_1^* < \frac{a_0}{a_1}$

The non-trivial steady state, x_e, when it exists, is uniquely determined and is locally and asymptotically stable, while the parasite-free steady state, x_{pf}, which always exists, is globally and asymptotically stable whenever $0 \le R_0 \le 1$ and unstable for $R_0 > 1$

$$
\begin{aligned}
&= -Aa_0 (1 - r_h)^2 + [-Aa_1 + Ba_1 - Ca_2] r_h m + [Ca_2 (1 - \sigma) - B + Da_4 \sigma] r_p \\
&\quad - Ca_2 \beta r_p m + [Aa_1 - Ca_3] m - [Da_4 - Ea_5] g_e - Ea_5 g_l \\
&= -Aa_0 (1 - r_h)^2 + [a_1 a_2 (1 - \sigma) - a_2] r_h m - Ca_2 \beta r_p m - a_3 m - Ea_5 g_l \\
&\le -Aa_0 (1 - r_h)^2 + [a_1 a_2 (1 - \sigma) - a_2] r_h m - Ca_2 \beta r_p m - a_3 m r_h - Ea_5 g_l, \\
&= -Aa_0 (1 - r_h)^2 - (a_2 + a_3) \left[1 - \frac{a_1 a_2 (1 - \sigma)}{a_2 + a_3} \right] r_h m - Ca_2 \beta r_p m - Ea_5 g_l, \\
&= -Aa_0 (1 - r_h)^2 - (a_2 + a_3) [1 - R_0] r_h m - Ca_2 \beta r_p m - Ea_5 g_l. \quad (60)
\end{aligned}
$$

Notice that the last term is negative whenever $R_0 \le 1$. In all we have the following: (i) $V' < 0$ if $R_0 \le 1$, for all t and $\forall x \in \mathcal{D}_0 \setminus \{(1, 0, 0, 0, 0)\}$; (ii) $V(x) = 0$ at $x = x_{pf}$ and (iii) $V(x) > 0$, $\forall x \in \mathcal{D}_0$ with $x \ne x_{pf}$. Thus, V is a positive definite function and $\{x_{pf}\}$ is the largest invariant compact subset in $\{x \in \mathcal{D}_0 | V' = 0\}$ containing only the equilibrium x_{pf} when $R_0 \le 1$, then by LaSalle's invariance principle, the parasite-free steady-state solution $x_{pf} = (1, 0, 0, 0, 0)$ of system (28)–(32) is globally asymptotically stable whenever $R_0 \le 1$. This ends the proof. $\square$

We note that the same function as defined in Eq. (58) with coefficients (59) would also suffice for the case where $g(r_h) = 1 - r_h$. However, a slight change would be required for the derivative of V^3, and with the compact region $\mathcal{D}_0$ redefined as

$$
\begin{aligned}
\mathcal{D}_0 = \Big\{ &(r_h, r_p, m, g_e, g_l) \in \mathbb{R}^5 : 0 \le r_h \le 1, 0 \le r_p \le r_p^\infty, 0 \le m \le m^\infty, \\
&0 \le g_e \le g_e^\infty, 0 \le g_l \le g_l^\infty \Big\}.
\end{aligned}
$$

The stability properties of the steady-state solutions of our system can be summarized as shown in Table 4.

---

[3] Here, $V' = -Aa_0 (1 - r_h)^2 \frac{1}{r_h} + (-Aa_1 + Ba_1 - Ca_2) r_h m + (Ca_2 (1 - \sigma) - B + Da_4 \sigma) r_p$.
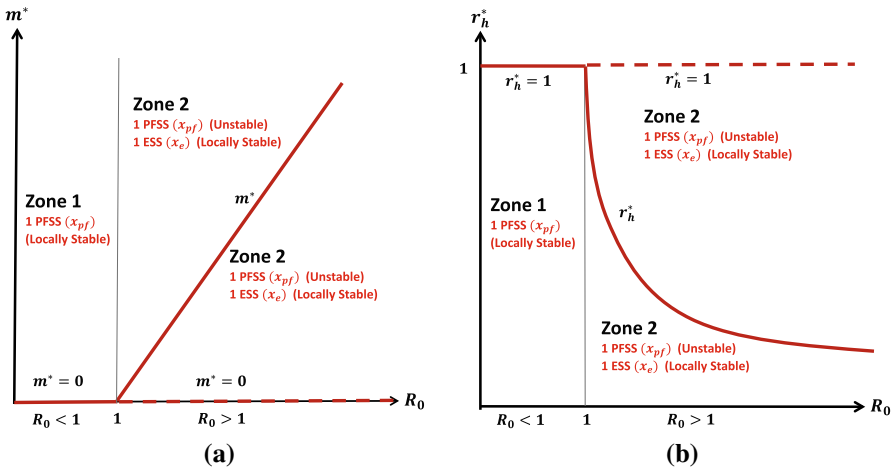
Fig. 4 Bifurcation plots of m^* (graph (a)) as defined in (39) and r_h^* (graph (b)) as defined in (38) against R_0 showing regions of existence and stability of the steady states for when $g(r_h)) = 1 - r_h$. Solid lines indicate stability and dash lines instability, determined by the size of R_0. The parasite-free steady state (PFSS) in the variables (r_h, r_p, m, g_e, g_l) is $x_{pf} = (1, 0, 0, 0, 0)$, and it always exist. It is stable (globally asymptotically) for $R_0 \leq 1$ and unstable for $R_0 > 1$. The parasitized steady state (ESS), x_e defined in (36) and (38), only exist for $R_0 > 1$, and when it does, it is stable. As we traverse from the zone $R_0 < 1$ to the zone $R_0 > 1$, there is a forward bifurcation occurring at $R_0 = 1$ (Color figure online)

Next, we characterize the existence and stability of the steady-state solutions as a function of R_0 in bifurcation diagrams. Figure 4 summarizes the results of the existence and stability of the steady states for the model with linear growth, $g(r_h) = 1 - r_h$, showing a forward bifurcation point occurring at $R_0 = 1$. The plots are for the steady state m^* and r_h^* of Eq. (38). Notice that the function m^* is a linear function of R_0, while r_h^* is of the form $\frac{\tilde{A}}{\tilde{A} + \tilde{B}(R_0 - 1)}$, a decreasing and concave up function, with $\tilde{A}$ and $\tilde{B}$ positive constants.

On the other hand, Fig. 5 summarizes the results of the existence and stability of the steady states for the recruitment function $g(r_h) = r_h(1 - r_h)$, also showing a forward bifurcation point occurring at $R_0 = 1$. The plots are for the steady state variables r_h^* of Eq. (39) and $m^* = m_1^*$ of Eqs. (40) and (41). In the proof of the existence of the steady state in Theorem 4 in Sect. 4.2.1, it was established that m_1^* increases with increase in R_0 from 1, at a decreasing rate, to its upper bound $\frac{a_0}{a_1}$. This produces a corresponding decrease in r_h^*.

4.3 Parasitemia Reproduction Number Using the Next-Generation Approach

In population models involving disease transmission, the term basic reproduction number, denoted by $\mathcal{R}_0$, is the average number of *secondary* infections produced by one primary infectious individual in a totally susceptible population during that infectious individual's period of infectiveness. In a population involving both susceptible and non-susceptible individuals, the term effective reproductive number, denoted $\mathcal{R}_{\text{eff}}$, is
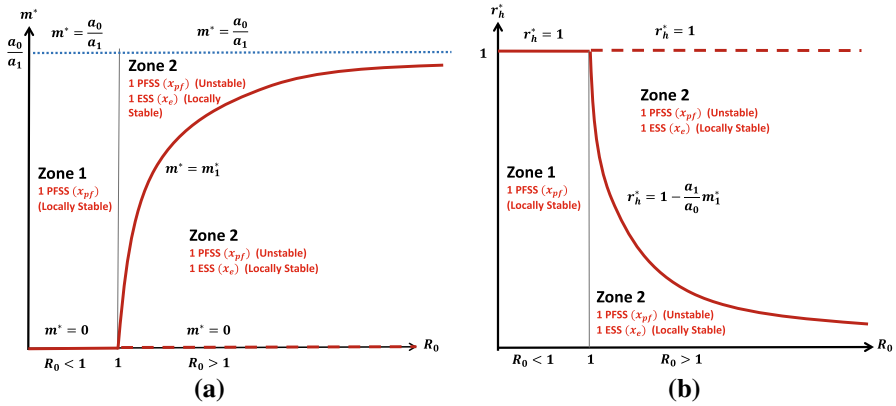
Fig. 5 Bifurcation plots of $m^* = m_1^*$ (graph (a)) defined in (42) and r_h^* (graph (b)) as defined in (39) against R_0 showing regions of existence and stability of the steady states for $g(r_h) = r_h(1 - r_h)$. Solid lines indicate stability and dash lines instability, determined by the size of R_0. The parasite-free steady state (PFSS) in the variables (r_h, r_p, m, g_e, g_l) is $x_{pf} = (1, 0, 0, 0, 0)$ always exists and is stable (globally asymptotically) for $R_0 \leq 1$ and unstable for $R_0 > 1$. The parasitized steady state (ESS), $x_e = (r_h^*(m_1^*), r_p^*(m_1^*), m_1^*, g_e^*(m_1^*), g_l^*(m_1^*))$ defined in (39) and (42), only exist for $R_0 > 1$, and when it does, it is stable. A forward bifurcation occurs at $R_0 = 1$ as we traverse from the $R_0 < 1$ to $R_0 > 1$ (Color figure online)

used to describe the average number of secondary cases produced per infectious case in this population (Ngonghala et al. 2015; Rothman et al. 2008), and it is bounded above by $\mathcal{R}_0$. In our current framework, the basic reproduction number, termed here, parasitemia reproduction number, quantifies the expected number of newly infected red blood cells produced by a single infected red blood cell at the onset of parasitemia. We will denote it by $\mathcal{R}_0$, and it determines whether parasitemia persists or not. If $\mathcal{R}_0 < 1$, each IRBC produces on average, less than one new IRBC, indicating the possibility of controlling parasitemia at some point. However, if $\mathcal{R}_0 > 1$, then there is persistence of parasitemia. Mathematically, it is the spectral radius of the next-generation matrix FV^{-1} (Driessche and Watmough 2002), where F is the matrix representing newly parasitized red blood cells and V is the matrix representing transfer terms, accounting for progression of IRBCs through the different stages of parasitemia.

To obtain the next-generation matrix, we first identify terms representing new infections in system (28)–(32) and separate them from the transfer terms. Let $\mathcal{F}_i$ be the rate of appearance of new IRBCs in compartment i, and let $\mathcal{V}_i^-$ be the rate of transfer of parasitized cells or free floating parasites out of compartment i and $\mathcal{V}_i^+$ be the rate of transfer into compartment i. Then, we can rewrite system (28)–(32) as $x' = \mathcal{F} - \mathcal{V} = [x_i']$, where $x = (x_1, x_2, x_3, x_4, x_5)^T = (r_h, r_p, m, g_e, g_l)^T$, is the vector of state variables, $x_i' = \mathcal{F}_i - \mathcal{V}_i$, $i = 1, 2, 3, 4, 5$, $\mathcal{F} = [\mathcal{F}_i]$, and $\mathcal{V} = [\mathcal{V}_i]$ with $\mathcal{V}_i = \mathcal{V}_i^- - \mathcal{V}_i^+$. Evaluating these matrices at the parasite-free steady state, $x_{pf} = (1, 0, 0, 0, 0)$ yields $F = \left[\frac{\partial \mathcal{F}_i}{\partial x_j}\right]$ and $V = \left[\frac{\partial \mathcal{V}_i}{\partial x_j}\right]$ for $i, j = 1, 2, \cdots, 5$. Then, the next-generation matrix is FV^{-1} and $\mathcal{R}_0 = \rho(FV^{-1})$. Applying this to system (28)–(32), in the variables (r_h, r_p, m, g_e, g_l), we have

$$\mathcal{F} = \begin{bmatrix} 0 \\ a_1 r_h m \\ 0 \\ 0 \\ 0 \end{bmatrix} \quad \text{and } \mathcal{V} = \begin{bmatrix} a_1 r_h m - a_0 g(r_h) \\ r_p \\ -a_2(1-\sigma)r_p + a_3 m + a_2(r_h + r_p)m \\ -a_4 \sigma r_p + a_4 g_e \\ -a_5 g_e + a_5 g_l \end{bmatrix}.$$

Then, their corresponding Jacobian matrices evaluated at the parasite-free steady state, $\mathbf{x}_{pf} = (1, 0, 0, 0, 0)$ yield F and V, where

$$F = \begin{pmatrix} 0 & 0 & 0 & 0 & 0 \\ 0 & 0 & a_1 & 0 & 0 \\ 0 & 0 & 0 & 0 & 0 \\ 0 & 0 & 0 & 0 & 0 \\ 0 & 0 & 0 & 0 & 0 \end{pmatrix} \quad \text{and } V = \begin{pmatrix} a_0 & 0 & a_1 & 0 & 0 \\ 0 & 1 & 0 & 0 & 0 \\ 0 & -a_2(1-\sigma) & a_2+a_3 & 0 & 0 \\ 0 & -a_4\sigma & 0 & a_4 & 0 \\ 0 & 0 & 0 & -a_5 & a_5 \end{pmatrix},$$

since $g'(1) = -1$ at the parasite-free steady state for both forms of $g(r_h)$. Hence,

$$V^{-1} = \begin{pmatrix} \frac{1}{a_0} & -\frac{a_1 a_2(1-\sigma)}{a_0(a_2+a_3)} & -\frac{a_1}{a_0(a_2+a_3)} & 0 & 0 \\ 0 & 1 & 0 & 0 & 0 \\ 0 & \frac{a_2(1-\sigma)}{a_2+a_3} & \frac{1}{a_2+a_3} & 0 & 0 \\ 0 & \sigma & 0 & \frac{1}{a_4} & 0 \\ 0 & \sigma & 0 & \frac{1}{a_4} & \frac{1}{a_5} \end{pmatrix}$$

$$\text{and } FV^{-1} = \begin{pmatrix} 0 & 0 & 0 & 0 & 0 \\ 0 & \frac{a_1 a_2(1-\sigma)}{a_2+a_3} & \frac{a_1}{a_2+a_3} & 0 & 0 \\ 0 & 0 & 0 & 0 & 0 \\ 0 & 0 & 0 & 0 & 0 \\ 0 & 0 & 0 & 0 & 0 \end{pmatrix}.$$

The dominant eigenvalue for FV^{-1} is the spectral radius $\rho(FV^{-1}) = \mathcal{R}_0 = \frac{a_1 a_2(1-\sigma)}{a_2+a_3} = R_0$.

Remark 4 The within-human–host malaria parasitemia reproduction number $\mathcal{R}_0$ obtained using the next-generation matrix matches the threshold value obtained in (37) that determined the existence and stability of the steady-state solutions in Theorems 4 and 5.

5 Numerical Simulation and Results

In this section, we carry out numerical simulation of the immune-suppressed model. The initial conditions used in the simulations are presented in Table 5. The initial number of HRBCs are based on estimates in Dean and National Center (2005), Hetzel and Anderson (1996), McKenzie and Bossert (1997), and we assume there are no IRBCs nor gametocytes to begin with. The initial number of merozoites is based on estimates of the number of hepatic schizonts produced per microlitre of blood, and

Table 5 Initial conditions

Variable	Description (Initial)	Range of values	Unit	Base value	References
$R_h(0)$	HRBC density	$[2 \times 10^5, 1 \times 10^7]$	C	2×10^6	Dean and National Center (2005), Hetzel and Anderson (1996) and McKenzie and Bossert (1997)
$R_p(0)$	IRBC density	0	C	0	Anderson et al. (1989) and Hetzel and Anderson (1996)
$M(0)$	Merozoite density	$[5 \times 10^{-3}, 4 \times 10^3]$	M	100	Baron (1996), Hetzel and Anderson (1996) and McKenzie and Bossert (1997)
$G_e(0)$	Immature gametocyte density	0	G	0	Bousema and Drakeley (2011) and Talman et al. (2004)
$G_l(0)$	Mature gametocyte density	0	G	0	Bousema and Drakeley (2011) and Talman et al. (2004)

The units of measurements are as earlier defined with C = Cell density $\times \mu l^{-1}$, M = Merozoite density $\times \mu l^{-1}$ and G = gametocyte density $\times \mu l^{-1}$ s

taking into account the proportion that survive at about 80% (McKenzie and Bossert 1997).

Using the parameters as stated in Table 3, we numerically simulate the model described by system (28)–(32), presenting the graphs in terms of the original variables. First, we present the results for the model in the absence of parasitemia, for both cases when the HRBC population is modelled by the linear growth function, $g(r_h) = (1 - r_h)$ and the logistic growth function, $g(r_h) = r_h(1 - r_h)$. Parameter values utilized are the base values stated in Table 3, with the parameter common to both models given by

$$\mu_h = 1/120, \ \beta_1 = \beta_2 = 6.5 \times 10^{-7}, \ \beta_3 = 0.75\beta_2, \ \mu_p = 0.0091, \gamma_p = 0.5,$$
$$r = 16, \ s = 1, \ \sigma = 0.1, \ \mu_m = 48, \ \mu_e = 0.28, \ \gamma_l = 0.15, \ \mu_l = 0.28.$$

Additionally, parameters specific to the choice of growth functions are $\Theta = 4.15 \times 10^4$, for the linear growth function with non-dimensional form $g(r_h) = (1 - r_h)$ and for the logistic growth function, $g(r_h) = r_h(1 - r_h)$, we have $\omega = \Lambda - \mu_h = 0.25$ where $\mu_h = 1/120$ as defined above and $\tilde{\mu}_h = 5 \times 10^{-8}$. Using these parameters, we obtain the basic reproduction numbers in the absence of parasitemia as $\mathcal{R}_0 \approx 0.894 < 1$ for the linear growth function and $\mathcal{R}_0 \approx 0.897 < 1$ for the logistic growth function.

With the base initial conditions, $R_h(0) = 2 \times 10^6$, $R_p(0) = 0$, $M(0) = 100$, $G_e(0) = 0$, $G_l(0) = 0$, (see Table 5), we obtain the profiles of the trajec-
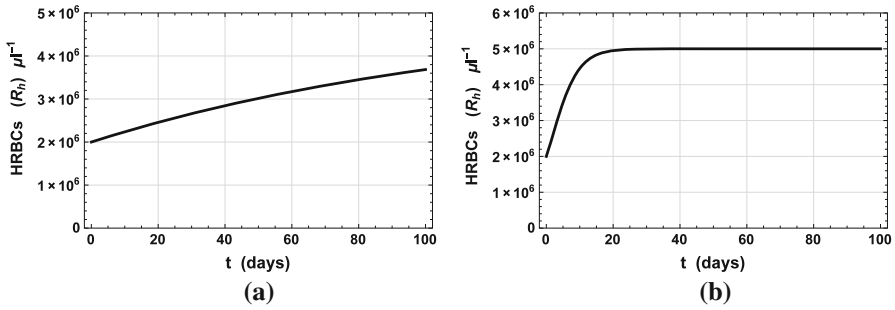
Fig. 6 Plots of HRBCs versus time showing the dynamics in the absence of Parasitemia. **a** Plots showing the trajectories when the linear growth function $F(R_h) = \Theta - \mu_h R_h$ is used. **b** Plots showing the trajectories when the logistic growth function $F(R_h) = (\Lambda - \mu_h)R_h - \tilde{\mu}_h R_h^2$ is used (Color figure online)
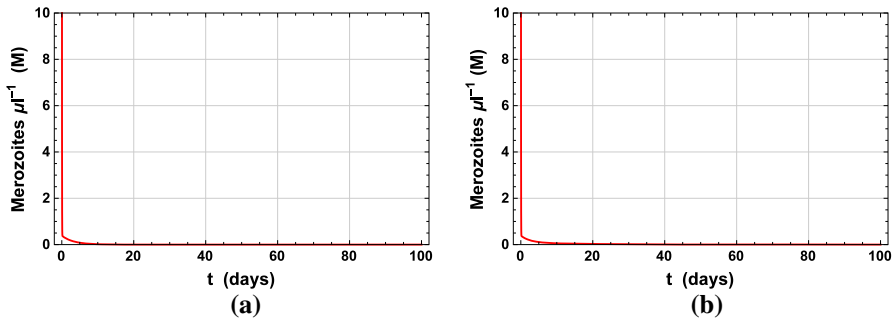

Fig. 7 Plots of free floating Merozoites versus time showing the dynamics in the absence of Parasitemia. **a** Plot showing the trajectories when the linear growth function $F(R_h) = \Theta - \mu_h R_h$ is used. **b** Plot showing the trajectories when the logistic growth function $F(R_h) = (\Lambda - \mu_h)R_h - \tilde{\mu}_h R_h^2$ is used (Color figure online)

tories in the absence of parasitemia presented in Figs. 6, 7 and 8 below. The profiles, plotted for the first 100 days, are very similar for both models. The solution curves converge to the parasite-free steady states $\mathbf{x}_{pf} = (\frac{\Theta}{\mu_h}, 0, 0, 0, 0)$ for the case when the non-dimensional linear growth function defined by $F(R_h) = \Theta - \mu_h R_h$ is used to model HRBCs recruitment, and $\mathbf{x}_{pf} = (\frac{\Lambda - \mu_h}{\tilde{\mu}_h}, 0, 0, 0, 0)$ for the case when a logistic growth function defined by $F(R_h) = (\Lambda - \mu_h)R_h - \tilde{\mu}_h R_h^2$ is used. However, the decay to zero for all disease-related state variables is faster for the linear model when compared with the logistic cases (see Fig. 8). Upon release from the liver, the effective initial released number of merozoites released infect HRBCs. However, the invasion is not sustainable as the merozoite density declines sharply leading to the eventual decay of the density of the IRBCs and gametocytes. Thus, the parasite is not able to establish parasitemia within the infected human. We note that similar profiles, just scaled appropriately, are obtained if a lower initial merozoite size is used.

In the presence of parasitemia, we maintain the same base parameters as in the parasite-free simulations, only changing σ (the proportion of infected red blood cells committed to gametocytogenesis), μ_p the death rate of infected red blood cells, β_1 (which in turn affects β_2 and β_3), the transmission rates. When β_1, hence β_2, is
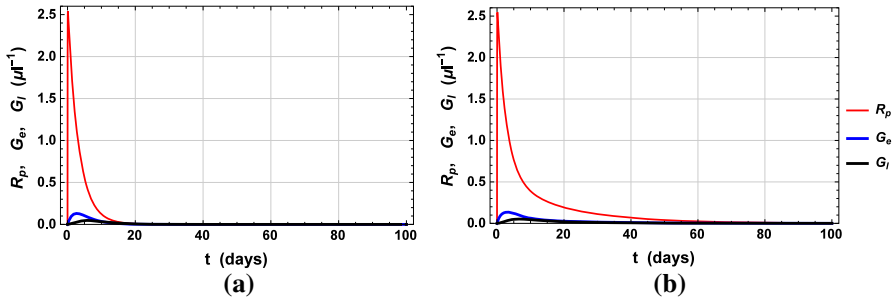
Fig. 8 Plots of infected red blood cells (IRBCs), early-state (immature) gametocytes and late-state (mature) gametocytes versus time in the absence of parasitemia. **a** Plot of trajectories when the linear growth function $F(R_h) = \Theta - \mu_h R_h$ is used. **b** Plots of trajectories when the logistic growth function $F(R_h) = (\Lambda - \mu_h)R_h - \tilde{\mu}_h R_h^2$ is used (Color figure online)
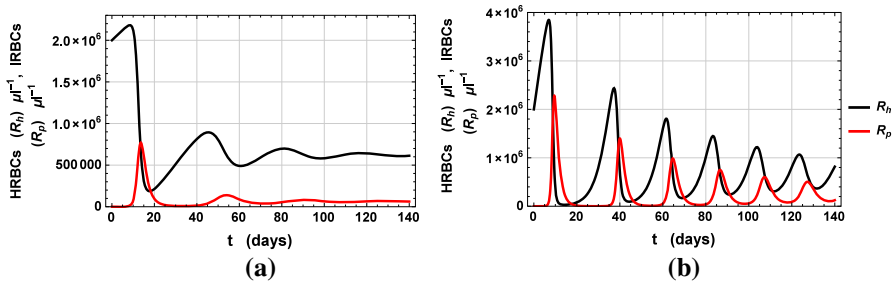

Fig. 9 Plots of HRBCs and IRBCs versus time showing the dynamics in the presence of parasitemia. **a** Plots showing the trajectories when the linear growth function $F(R_h) = \Theta - \mu_h R_h$ is used. **b** Plots showing the trajectories when the logistic growth function $F(R_h) = (\Lambda - \mu_h)R_h - \tilde{\mu}_h R_h^2$ is used (Color figure online)

increased from 6.5×10^{-7} to 6.0×10^{-6}, σ reduced from 0.1 to 0.0064, and μ_p increased from 0.0091 to 0.07, with all other parameters kept unchanged, the parasite succeeds to invade the human system and establishes itself within an infected human. The corresponding basic reproduction numbers in the presence of parasitemia are now $\mathcal{R}_0 \approx 5.350 > 1$ for the linear growth function and $\mathcal{R}_0 \approx 5.364 > 1$ for the logistic growth function. Starting with an initial merozoite density of 10 per μL of blood, and maintaining the other base initial conditions the same as in the parasite-free model, we obtain the profiles of the trajectories in the presence of parasitemia, plotted for 140 days and presented in Figs. 9, 10 and 11. We note that the effect of a larger merozoite initial number (say 100 per μL), with all other parameters and initial conditions held fixed were very minimal and not noticeable.

Figures 9, 10 and 11 show oscillatory dynamics reminiscent of malaria parasitemia in humans. The oscillations approach a stable parasite steady state. These oscillatory trajectories are likely due to the cyclic pattern in the within-human–host parasite life cycle that results in the periodic destruction of healthy red blood cells, eventually replenished from the bone marrow. This destruction is as a result of merozoites infecting the healthy red blood cells resulting in a dwindling in their numbers and that of
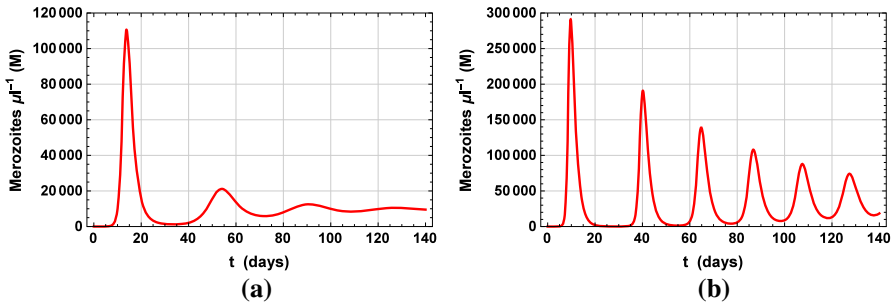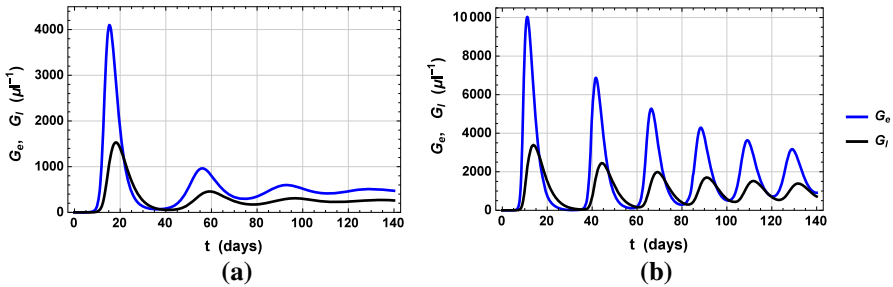
Fig. 10 Plots of free floating Merozoites vs time showing the dynamics in the presence of parasitemia. **a** Plot showing the trajectories when the linear growth function $F(R_h) = \Theta - \mu_h R_h$ is used. **b** Plot showing the trajectories when the logistic growth function $F(R_h) = (\Lambda - \mu_h)R_h - \tilde{\mu}_h R_h^2$ is used (Color figure online)

Fig. 11 Plots of early-state (immature) and late-state (mature) gametocytes vs. time in the presence of parasitemia. **a** Plots showing the trajectories when the linear growth function $F(R_h) = \Theta - \mu_h R_h$ is used. **b** Plots showing the trajectories when the logistic growth function $F(R_h) = (\Lambda - \mu_h)R_h - \tilde{\mu}_h R_h^2$ is used (Color figure online)

the healthy red blood cells. However, it leads to an increase in the parasitized red blood cells. After a few days, the parasitized red blood cells, not committed to the gametocyte path, rupture releasing more free floating merozoites, thereby increasing the number of free floating merozoites available to infect more healthy red blood cells. This increase–decrease is captured by the oscillatory dynamics in our result.

Comparing the profiles from the linear model (Figs. 9, 10 and 11 graphs (a)) to those corresponding to the logistic model (Figs. 9, 10 and 11 graphs (b)), we see that the oscillatory trajectories for the logistic model occur more frequently than those from the linear model, when the same parameter sets are used, except the net recruitment terms. The first peak occurred some more than 10–12 days after the initial invasion of health red blood cells by merozoites.

We note that the total gametocyte densities (see Figs. 11a, b), determined by the area under the gametocyte density curves, are much higher than what has been reported to be observed in malaria patients in nature. The gametocyte density in patients has been observed to fall in the range 2–60 gametocytes per μL in asymptomatic infections and up to 1000 gametocytes per μL of blood in symptomatic infections (see Baton and Ranford-Cartwright (2005), Mitri et al. (2009) and Teboh-Ewungkem and Yuster (2010) with the references therein. This value can increase or decrease depending on

the transmission season, the age of the malaria patient and the transmission region, whether a low or high transmission region. The latter two conditions are correlated with the level of immunity by the individuals living in a region. Since our analysis was carried out for the immune-suppressed model, one would expect higher overall gametocyte densities in this case as the natural control factor, the immune system is absent. We are currently investigating the role of immunity, innate and adaptive, in reducing the size of this gametocyte load.

Our numerical simulations when $R_0 > 1$ (Figs. 10 and 11) indicate that it is possible to have long-term endemic parasitemia. This is because there are no controls in the model. One would expect fadeout with the inclusion of immunity and/or the use of prophylaxes. To destroy the stable steady state and lower parasite loads or achieve control of the malaria disease with an infected patient, immediate intervention would be necessary, especially in the naive immune individuals, the limiting case with no immunity analysed in this manuscript.

6 Discussion and Conclusion

In this manuscript, we have developed a model for the dynamics of the malaria parasites within the human–host. Our model takes into account both innate and adaptive immunity and views the process of gametocytogenesis as a developmental pathway through the formation of early-state gametocytes through maturation to the late-state gametocytes. We hypothesized that it is these late-state gametocytes that can be picked up by the female *Anopheles sp* mosquito when it takes a blood meal from the infected human host. Now, an assumption often made in the analyses of the dynamics of many epidemic models is that the duration of immunity is independent of exposure to infection (Anderson and May 1979, 1991; Hethcote et al. 1982). However, the immunity to malaria has, for sometime now, been known to be sustained by continuing exposure (Aron 1983, 1988a), and that as far as malaria is concerned, the conventional definition of immunity as absolute refractoriness to infection may be restrictive, as immunity may confer protection against severe clinical illness without eliminating chronic, mild infections (Aron 1988b). That is, asymptomatic immune malaria carriers can be infective. This phenomenon of incomplete immunity permitting disease transmission is known to exist for malaria and complicates disease control strategies as the reservoir of infection now includes symptomatic and asymptomatic infected individuals. To address this issue of incomplete immunity in our model, we considered two types of immune responses: the innate and adaptive immune response of the system to the infection. These two types of immune responses are modelled on the assumption that the innate immune state of the human individual is always available and serves as the first line guard against all types of infections that invade the human body. Thus, its effect on the system is more permanent. On the other hand, it is assumed that the adaptive immune response is predicated on the fact that the additional immunity to malaria is sustained by continuing exposure to the malaria infection, so that this adaptive-type immunity is triggered by onset of the infection in the body and wanes away over time in the absence of the infection. We have hypothesized that it is the interplay between adaptive and innate immunity that work together in the human leading to the

phenomenon where asymptomatic immune individuals are protected against severe morbidity and illness due to infection by malaria, but allows the individual to harbour parasite loads that permit transmission. The result of the interplay between innate and adaptive immunity in the presence of a infection and red blood cell growth is captured in a nonlinear system of autonomous ordinary differential equations, whose form and provenance are carefully explained and displayed in Sect. 2 of the manuscript. The model addressed aspect of malaria parasitemia and gamete formations in a manner which we believe is simple and revealing. To the best of our knowledge, we think this is probably the only ordinary differential equations within-host malaria model thus far that explicitly incorporates the late-state gametocytes, the actual transmissible and infectious forms of the parasites, as well as incorporate both the innate immune effects and the adaptive immune effects in the model development in the way it has been done in the current manuscript.

Mathematically, the analyses to establish the well-posedness, boundedness and positivity of the general model equations with innate and adaptive immune effects incorporated were carried out. Subsequently, a complete analysis of the model under the simplifying assumption of immune suppression has been presented. The main objective of the current analysis was to understand the role that the choice of the recruitment function plays on the within-human–host parasite dynamics. To achieve this objective, two healthy red blood cell recruitment functions were considered: a constant recruitment function and a logistic recruitment function. Our analysis indicated the existence of a parasite threshold parameter, R_0, whose size determined the existence and stability of steady states. Regardless of choice of recruitment function, the model admits a parasite-free steady state which exists for all R_0 values, but is globally stable for $R_0 \leq 1$, and is unstable when $R_0 > 1$. However, the logistic model also admits an additional trivial equilibrium which exists and is unstable for all R_0 values. When $R_0 > 1$, both models admit additional parasitized steady-state solutions. The parasitized steady-state solutions in the case of the constant recruitment model that exists, are unique and locally stable whenever $R_0 > 1$. On the other hand, for the logistic model, when $R_0 > 1$, the mathematical equations point towards the existence of two parasitized steady-state solutions, but with the required condition for existence (and stability) of a biologically feasible solution being that the merozoite steady-state population size be bounded by some threshold value, beyond which a parasitized steady state no longer is realistic, in the sense that the healthy red blood cells would have completely been depleted at this point. Therefore, only one of the parasitized steady state fulfils the feasibility criteria; the other results in a scenario where the healthy red blood cells have undergone massive destruction leading to their total elimination. The massive destruction of red blood cells can cause a malaria patient to become severely anaemic which can lead to a malaria infection complication known as blackwater fever, also called malarial haemoglobinuria. This is a severe, potentially highly fatal, complication from *Plasmodium falciparum* malaria infection whereby haemoglobin is released into the blood stream and can be found in urine and kidney due to the massive and extensive destruction of the red blood cells as the parasites progressively break down more healthy red blood cells.

In most mathematical models of the within-human–host dynamics of the malaria parasite, analysis of the model usually indicates the existence of two or more steady

states when $R_0 > 1$. Our model's dynamics indicate that this conclusion is not quite trivial. We have analytically shown that although there may be situations pointing to the existence of more than one parasitized steady states, further analysis is required and may show otherwise. In particular, we showed in our model that for the logistic model, although there were two positive parasitized steady states, one of them led to the complete depletion of the healthy red blood cells, a parasite take-over scenario, which is potentially fatal if no immediate and strict control measures are enacted in the affected patients. This conditioned depletion of healthy red blood cells by malaria parasitemia is predicted by our analysis of the immune-suppressed model (the scenario that can arise in the first attack on an individual from a non-malaria zone to malarious zone). We have therefore set the stage to investigate how the action of innate immunity and the triggering of adaptive immune response will affect the within-human–host dynamics of the malaria parasite. Thus, the analysis of the full model in the presence of a functional innate and adaptive immune system is the subject of future work. One would expect that immunity (innate and or adaptive) should lower parasitemia loads and peaks as well as regulate the size of the parameter window within which complete red blood cell depletion during malaria parasitemia is possible. Thus, the effects of adaptive and innate immune responses on infected humans (symptomatic or asymptomatic) and how they impact parasitemia and the size of the threshold parameter, are currently being investigated. We have not yet presented a complete sensitivity analysis of the effect of the different parameters in our model on the onset of gametocytes as well as the build-up of adaptive immunity to malaria infections in endemic areas. These and the other aspects discussed in our model including the possibility whereby the magnitude of the effects of invasion of HRBCs by merozoites may be different from the magnitude of the effects of absorption of the merozoites by the HRBCs (different contact rates) are subject currently being investigated. Though more biological investigation is needed for a full characterization of the phenomena of gametocytogenesis and contact rates between different cell types in the body, we are aiming at providing a mathematical and theoretical characterization.

Appendix

Positivity and Positive Invariance Solution

Theorem 7 (Statement of the positivity and positive invariance of solution theorem)
Consider system (8)–(14) *with initial conditions in* (15) *and under the conditions given for* $\psi(R_h)$ *and* $H_i(E_i)$ *as stated in Sect.* 2.2. *Then, every solution of the system with initial condition in* $\mathbb{R}_+^7$ *remains in* $\mathbb{R}_+^7$. *Additionally, if* $\boldsymbol{x}(0) \equiv \boldsymbol{0}$, *the solution of system* (8)–(14) *will remain zero (or positively bounded depending on the form of* $\psi(R_h)$), *for all time* $t > 0$. *That is,* $\mathbb{R}_+^7$ *is positively invariant and attracting with respect to the system. Furthermore, the system has a forward positive solution in* $\mathbb{R}_+^7$ *provided that it starts in it.*

Proof We show that the region $\mathbb{R}_+^7$ is positively invariant, that is, whenever $\boldsymbol{x}(0) \in \mathbb{R}_+^7$, $\boldsymbol{x} \in \mathbb{R}_+^7$, $\forall t \geq 0$. It suffices to show that there is no solution of the system starting in $\mathbb{R}_+^7$ which is non-positive. Thus, we are required to show that the rate of change of each state variable, that is each ϕ_i, $1 \leq i \leq 7$, is non-negative at the origin $\boldsymbol{0} = (0, 0, 0, 0, 0, 0, 0)$, and on each of the coordinate axis. Notice that at the origin $\boldsymbol{0}$, if $\boldsymbol{x}_0 = \boldsymbol{0}$, then $\boldsymbol{x}'(0) = \Phi(\boldsymbol{0}) = \boldsymbol{0}$ if $\psi(R_h) = \Lambda - \tilde{\mu}_h R_h$, or $\boldsymbol{x}'(0) = (\Theta, 0, 0, 0, 0, 0, 0)$ if $\psi(R_h) = \frac{\Theta}{R_h}$. Thus, if $\boldsymbol{x}(0) = \boldsymbol{0}$, each component of $\boldsymbol{x}$ remains stationary at zero or increases from zero depending on the form of ψ. On the other hand, if any one of the components of $\boldsymbol{x}$ is zero, the rate of change of that component with time is non-negative, showing that no trajectory of the system passes out of $\mathbb{R}_+^7$ through that component's zero axes. For example, when $R_p = 0$, $R_p' = \frac{\beta_1 R_h M}{1 + \xi_0 E_a} \geq 0$, since R_h and M are non-negative for all time, showing that no solution of the system passes out of $\mathbb{R}_+^7$ through the $R_p = 0$ axis. This implies the vector field of the system is inward pointing on the boundary of $\mathbb{R}_+^7$. That is, if $\boldsymbol{x}_0 \in \mathbb{R}_+^7$, then $\boldsymbol{x} \in \mathbb{R}_+^7$, $\forall t \geq 0$. Therefore, the region $\mathbb{R}_+^7$ is positively invariant and attracting.

Next to prove the *positivity* of the solution, we follow the steps in Ngwa et al. (2016), Page 8. Suppose there exists $t_1 > 0$ such that $R_h(t_1) = 0$, $R_h'(t_1) < 0$ and $R_h, R_p, M, G_e, G_l, E_i, E_a > 0$ for all $0 < t < t_1$. Then

$$R_h'(t_1) = \underbrace{R_h(t_1)\psi(R_h(t_1))}_{:=\psi_0} - \underbrace{\mu_h R_h(t_1)}_{:=0} - \underbrace{\frac{\beta_1 R_h(t_1) M(t_1)}{1 + \xi_0 E_a(t_1)}}_{:=0} = \begin{cases} \Theta & \text{if } \psi(R_h) = \frac{\Theta}{R_h} \\ 0 & \text{if } \psi(R_h) = \Lambda - \tilde{\mu}_h R_h. \end{cases}$$

In either case, $R_h'(t_1) \geq 0$, leading to a contradiction to the assumption that $R_h'(t_1) < 0$. So, no such t_1 exists, and hence $R_h \neq 0$. Thus, $R_h(t) > 0$, $\forall t \geq 0$. Next suppose that there exists t_2 such that $R_p(t_2) = 0$, $R_p'(t_2) < 0$ and $R_h, R_p, M, G_e, G_l > 0$ for all $0 < t \leq t_2$. Then, $R_p'(t_2) = \frac{\beta_1 R_h(t_2) M(t_2)}{1 + \xi_0 E_a(t_2)} - \underbrace{(\gamma_p + \mu_p) R_p(t_2)}_{:0} = \frac{\beta_1 R_h(t_2) M(t_2)}{1 + \xi_0 E_a(t_2)} > 0$, which is a contradiction to the assumption that $R_p'(t_2) < 0$. Hence, $R_p(t) > 0$, $\forall t > 0$. Similarly, one can show that $M(t) > 0$, $G_e(t) > 0$, $G_l(t) > 0$, $E_i(t) > 0$ and $E_a(t) > 0$ for all $t > 0$. Therefore, any solution of the system with an initial condition in $\mathbb{R}_+^7$ is positive. $\qquad\square$

Boundedness of Solution

Theorem 8 (Statement of the boundedness of solution theorem) *Consider system* (8)–(14) *with initial conditions in* (15) *and under the conditions for* $\psi(R_h)$ *and* $H_i(E_i)$ *as stated in Sect.* 2.2. *Then, every forward solution of the system in* $\mathbb{R}_+^7$, *with initial condition in* $\mathbb{R}_+^7$, *is bounded. Moreover, the system is uniformly dissipative in* $\mathbb{R}_+^7$.

Proof To start the proof of boundedness, we first note the following about boundedness of $f(R_h)$ and $H_i(E_i)$.

1. For all values of R_h, we have

$$R_h \psi(R_h) \leq \mathcal{K}_{\mathcal{R}}, \text{ where } \mathcal{K}_{\mathcal{R}} = \begin{cases} \Theta & \text{if } \psi(R_h) = \frac{\Theta}{R_h} \\ \frac{\Lambda^2}{4\tilde{\mu}_h} & \text{if } \psi(R_h) = \Lambda - \tilde{\mu}_h R_h. \end{cases} \quad (61)$$

We note that the requirement that ψ be monotone non-increasing tacitly comes along with the requirement that $R_h \psi(R_h)$ be continuous from right at the origin. In particular, $\psi(R_h)$ satisfies conditions (1)–(3) of Sect. 2.2. Other examples, besides the two studied in this manuscript, of recruitment functions $\psi(R_h)$ found in the biological literature that satisfy conditions (1)–(3) of Sect. 2.2 are $\psi(R_h) = \Lambda e^{-\tilde{\mu}_h R_h}$, Ricker recruitment function and $\psi(R_h) = \frac{\Lambda}{1+\left(\frac{R_h}{L}\right)^n}$, $\Lambda, L, n, \tilde{\mu}_h > 0$ which is the Maynard–Smith–Slatkin function. Details on these types of recruitment functions can be found in Brännström and Sumpter (2005) and Ngonghala et al. (2016).

2. Similarly, for all values of E_i we have

$$H_i(E_i) \leq \mathcal{K}_i \text{ where } \mathcal{K}_i$$
$$= \begin{cases} \frac{\delta_i K_i}{4} & \text{if } H(E_i) = \delta_i E_i \left(1 - \frac{E_i}{K_i}\right) \\ \max(A_1, A_2, 0) & \text{if } H_i(E_i) = \delta_i E_i \left(1 - \frac{E_i}{K_i}\right)\left(\frac{E_i}{M_i} - 1\right) \end{cases} \quad (62)$$

where on setting $B = -K_i M_i + K_i^2 + M_i^2 = \left(M_i - \frac{1}{2}K_i\right)^2 + \frac{3}{4}K_i^2 > 0$ we can obtain

$$A_1 = \frac{\delta_i\left(-\sqrt{B} + K_i - 2M_i\right)\left(-\sqrt{B} + K_i + M_i\right)\left(\sqrt{B} + 2K_i - M_i\right)}{27 K_i M_i}$$

$$A_2 = -\frac{\delta_i\left(\sqrt{B} + K_i - 2M_i\right)\left(\sqrt{B} - 2K_i + M_i\right)\left(\sqrt{B} + K_i + M_i\right)}{27 K_i M_i}.$$

Thus, the functions H_i and $R_h \psi$ defined are bounded.

Now to prove the boundedness of the R_h and R_p, let $R(t) = R_h(t) + R_p(t)$ be the total size of red blood cells within the human at time t, (healthy plus infected red blood cells) with $R(0) = R_h(0) + R_p(0) = R(0)$. Then, we have from the first two equations of system (8)–(14)

$$\frac{\mathrm{d}R}{\mathrm{d}t} = R_h \psi(R_h) - \mu_h R_h - (\gamma_p + \mu_p)R_p - (\rho_p + \rho_a E_a)R_p E_i$$
$$\leq f(R_h) - \mu R, \text{ where } \mu = \min(\mu_h, \gamma_p + \mu_p),$$

where $f(R_h) = R_h \psi(R_h)$ with $\psi : [0, \infty) \to \mathbb{R}_+$ a monotone decreasing continuously differentiable function. So, the function $f : [0, \infty) \to \mathbb{R}_+$ has a maximum value which is either constant when f is the constant function, or that occurs at the point $R_h^* \in [0, \infty)$, where R_h^* satisfies the equation $f'(R_h^*) = \psi(R_h^*) + R_h^* \psi'(R_h^*) = 0$. Set $\mu = \min(\mu_h, \gamma_p + \mu_p)$ and suppose that the maximum value of f is $\mathcal{K}_R$, then we have from above,

$$\frac{\mathrm{d}R}{\mathrm{d}t} + \mu R \leq \mathcal{K}_R \Rightarrow R(t) \leq \frac{\mathcal{K}_R}{\mu} + Ae^{-\mu t},$$

where A is an arbitrary constant that can be determined from initial data. Observe that if the initial condition, $R(0)$, is such that $R(0) > \frac{\mathcal{K}_R}{\mu}$, then A is always positive and the bound for $R(t)$ is decreasing with time. When $R(0) = \frac{\mathcal{K}_R}{\mu}$, then A is non-negative and the bound for $R(t)$ is non-increasing with time. Finally, if $R(0) < \frac{\mathcal{K}_R}{\mu}$, A can be a negative number and the bound for $R(t)$ will be an increasing function of t. If at any of the instances we see that

$$\lim_{t \to \infty} \sup R(t) \leq \frac{\mathcal{K}_R}{\mu}. \tag{63}$$

Thus, $0 \leq R_h(t) + R_p(t) \leq \frac{\mathcal{K}_R}{\mu}$, $\forall t \geq 0$. So there exist R_h^∞ and R_p^∞ with the property that $0 \leq R_h(t) \leq R_h^\infty$ and $0 \leq R_p(t) \leq R_p^\infty$, $\forall t \geq 0$. Hence, R_h and R_p are bounded solutions.

Next we consider the equation for M, namely,

$$\frac{\mathrm{d}M}{\mathrm{d}t} = \frac{r\gamma_p(1-\sigma)R_p}{1 + \xi_1 E_a(t)} - \mu_m M - \left(\frac{\beta_2 R_h}{1 + \xi_0 E_a} + \frac{\beta_3 R_p}{1 + \xi_0 E_a} + (\rho_m + \rho_n E_a)E_i\right)M,$$

and observe that when we take into consideration the fact that the quantity $\frac{1}{1+\xi_1 E_a}$ is largest when $E_a = 0$, we have that

$$\frac{\mathrm{d}M}{\mathrm{d}t} \leq r\gamma_p(1-\sigma)R_p^\infty - \mu_m M \Rightarrow M(t) \leq \frac{r\gamma_p(1-\sigma)R_p^\infty}{\mu_m} + Be^{-\mu_m t},$$

where B is an arbitrary constant. As above we arrive at the conclusion that there exist M^∞ such that $0 \leq \sup M(t) \leq M^\infty$, $\forall t \geq 0$. So M is bounded.

Next to prove the boundedness of G_e and G_l, we set $G(t) = G_e(t) + G_l(t)$ to be the total size of gametocytes within the human and see that

$$\frac{\mathrm{d}G}{\mathrm{d}t} = \frac{s\sigma\gamma_p R_p}{1 + \xi_1 E_a} - (\gamma_l + \mu_e)G_e - (\rho_g + \rho_q E_a)G_e E_i + \frac{\gamma_l G_e}{1 + \xi_1 E_a} - \mu_l G_l - \rho_l E_i G_l$$
$$\leq s\sigma\gamma_p R_p^\infty - \min(\mu_e, \mu_l)G.$$

Thus

$$\frac{\mathrm{d}G}{\mathrm{d}t} + \min(\mu_e, \mu_l)G \leq r\sigma\gamma_{p,m}R_p^\infty \Rightarrow G(t) \leq \frac{r\sigma\gamma_{p,m}R_p^\infty}{\min(\mu_e, \mu_l)} + Ce^{-\min(\mu_e, \mu_l)t}.$$

Therefore, as before, there exist G_i^∞ and G_e^∞ with the property that for $0 \leq G_e(t) \leq G_e^\infty$ and $0 \leq G_l(t) \leq G_l^\infty, \forall t \geq 0$. So G_e and G_l are bounded whenever the preceding variables are bounded.

To establish boundedness of the solutions for the equations of the innate and adaptive immune responses, we proceed as follows. From the last two equations of the general model, system (8)–(14), and using the above results, we get

$$\frac{\mathrm{d}E_i}{\mathrm{d}t} + \left(\lambda_1 R_p^\infty + \lambda_2 M^\infty\right) E_i \leq \mathcal{K}_i + \vartheta_1 R_p^\infty + \vartheta_2 M^\infty$$

$$\frac{\mathrm{d}E_a}{\mathrm{d}t} + \left(\mu_a + \theta_1 R_p^\infty + \theta_2 M^\infty)\right) E_a \leq \varrho_1 R_p^\infty + \varrho_2 M^\infty,$$

with the right hand side here being only constants and we can again argue as above to come to the conclusion that each E_i will show bounded growth whenever M, R_h and R_P are bounded. This completes the prove for boundedness. So, if we let

$$B^\infty = \max\{R_h^\infty, R_h^\infty, M^\infty, G_e^\infty, G_l^\infty, E_i^\infty, E_a^\infty\},$$

then each of R_h, R_p, M, G_e, G_l, E_i, $E_a \leq B^\infty$. In the absence of disease, system (8)–(14) reduces to the decoupled equations for the healthy red blood cell population and for the immune cells as follows:

$$\frac{\mathrm{d}R_h}{\mathrm{d}t} = R_h\psi(R_h) - \mu_h R_h, \quad \frac{\mathrm{d}E_i}{\mathrm{d}t} = H_i(E_i), \quad \frac{\mathrm{d}E_a}{\mathrm{d}t} = -\mu_a E_a.$$

Note here that in the absence of Allee effect, $H_i(E_i)$ can have similar forms as $F(R_h)$. That is, we can write

$$H_i(E_i) = E_i\varphi(E_i) - \mu_i E_i,$$

where $\varphi : [0, \infty) \to \mathbb{R}_+$ is a function defined similarly as ψ and satisfies the conditions stated for ψ.

So, to prove the boundedness of these functions we observe that the equation for the healthy red blood cell population then satisfies the relation

$$\frac{\mathrm{d}R_h}{\mathrm{d}t} = R_h\psi(R_h) - \mu_h R_h \Rightarrow t(R_h) = \int \frac{1}{R_h(\psi(R_h) - \mu_h)}\mathrm{d}R_h + C,$$

where C is an arbitrary constant of integration. For the functional forms of ψ used here, if at time $t = 0$, $R_h(t) = R_{0h}$, we have

$$t(R_h) = \begin{cases} \frac{1}{\mu_h} \ln\left(\frac{\Theta - \mu_h R_{0h}}{\Theta - \mu_h R_h}\right) & \text{if } \psi(R_h) = \frac{\Theta}{R_h} \\ \frac{1}{\omega} \ln\left(\frac{R_h(R_{0h} - K)}{R_{0h}(R_h - K)}\right) & \text{if } \psi(R_h) = \Lambda - \tilde{\mu}_h R_h \end{cases},$$

where $\omega = \Lambda - \mu_h$ and $K = \frac{\omega}{\mu_h}$. For both forms of recruitment, it is clear that $t(R_h) \to \infty$ when $R_h \to \Theta/\mu_h$ or $R_h \to K$, respectively. So the solutions remain bounded. Also, in the absence of disease, the expression for the innate immunity at any time can be written as an exact integral. That is

$$\frac{dE_i}{dt} = H_i(E_i) \Rightarrow t(E_i) = \int \frac{1}{H_i(E_i)} dE_i + C, \tag{64}$$

where C is a constant whose values can be determined by the initial conditions. So,

$$t(E_i) = \begin{cases} \frac{K_i(\ln(E_i - M_i) - \ln(E_i)) + M_i(\ln(E_i) - \ln(E_i - K_i))}{\delta_i(K_i - M_i)} + C & \text{if } H_i(E_i) = E_i \delta_i \left(1 - \frac{E_i}{K_i}\right)\left(\frac{E_i}{M_i} - 1\right) \\ \frac{\ln(E_i) - \ln(E_i - K_i)}{\delta_i} + C & \text{if } H_i(E_i) = E_i \delta_i \left(1 - \frac{E_i}{K_i}\right) \end{cases},$$

so that if at time $t = 0$, $E_i(0) = E_{0i}$, we have the implicit solution

$$t(E_i) = \begin{cases} \frac{1}{\delta_i(K_i - M_i)} \ln\left(\left(\frac{E_{0i}(E_i - M_i)}{E_i(E_{0i} - M_i)}\right)^{K_i} \left(\frac{E_i(E_{0i} - K_i)}{(E_i - K_i)E_{0i}}\right)^{M_i}\right) & \text{if } H_i(E_i) = E_i \delta_i \left(1 - \frac{E_i}{K_i}\right)\left(\frac{E_i}{M_i} - 1\right) \\ \frac{1}{\delta_i} \ln\left(\frac{E_i(E_{0i} - K_i)}{E_{0i}(E_i - K_i)}\right) & \text{if } H_i(E_i) = E_i \delta_i \left(1 - \frac{E_i}{K_i}\right) \end{cases}$$

We then see clearly that for the logistic case, $t \to \infty$ whenever $E_i \to K_i$ for any starting value of $E_{0i} > 0$. In the case with the Allee effect, if $0 < M_i < K_i$ then $0 < E_{0i} < M_i$, $t(E) \to \infty$ as $E_i \to 0+$, while if $E_{0i} > M_i$, then again, $t(E) \to \infty$ as $E_i \to K_i$. This shows that in either case, the solutions remain bounded. The inverse function theorem can be applied to obtain the solution $E_i(t)$ in some special cases of values of M_i and K_i. We have thus established boundedness of the solutions in all cases in both the presence and absence of the infection. $\square$

Uniqueness of Solution

Theorem 9 (Statement on the Uniqueness of Solution) *The positive and bounded solution for the system* (8)–(14) *whenever it exists, is unique.*

Proof We show that the function Φ defined above is globally Lipschitz in $\mathbb{R}_+^7$ and hence the equation $x'(t) = \Phi(x(t))$, $x(0) = x_0$ has a unique solution. It is clear that $\mathbb{R}_+^7$ is a convex set, Φ is continuously differentiable, since the partial derivatives $\frac{\partial \Phi}{\partial x_i}$, $i = 1, 2, \ldots, 7$ exist, and are continuous. We show that these partial derivatives are bounded in $\mathbb{R}_+^7$: Since $R_h \psi(R_h)$ is monotone decreasing, continuously differentiable function and each state variable R_h, R_p, M, G_e, G_l, E_i, E_a are continuously differentiable, then each component Φ_i, $i = 1, 2, 3 \ldots, 7$ of the vector valued function Φ on right hand side of system (8)–(14) exists and are continuously differentiable because they are rational functions of the state variables. It suffices to

show that $\|\frac{\partial \Phi}{\partial x_i}\|_\infty$ $i = 1, 2, \cdots, 7$ are bounded where $(x_1, x_2, x_3, x_4, x_5, x_6, x_7) = (R_h, R_p, M, G_e, G_l, E_i, E_a)$. Observe, for example, that

$$\left\|\frac{\partial \Phi}{\partial R_h}\right\|_\infty = \max\left\{\left|\frac{\partial \phi_i}{\partial R_h}\right|, i = 1, 2, \ldots, 7\right\}$$

$$= \max\left\{\left|\psi(R_h) + R_h\psi'(R_h) - \mu_h - \frac{\beta_1 M}{1 + \xi_0 E_a}\right|, \left|\frac{\beta_1 M}{1 + \xi_0 E_a}\right|, 0, 0, 0, 0, 0\right\}$$

$$\leq \left|\psi(R_h)\right| + R_h\left|\psi'(R_h)\right| + \left|\mu_h + \frac{\beta_1 M}{1 + \xi_0 E_a}\right|$$

$$\leq B_1$$

for some B_1, since M and E_a are bounded, and ψ is monotone decreasing so that $|\psi'|$ is monotone increasing and bounded by say K where K is the carrying capacity for R_h, so B_1 exists. Similarly, there exists $B_i < \infty$, for $i = 2, 3, \cdots, 7$ such that

$$\left\|\frac{\partial \Phi}{\partial R_p}\right\|_\infty = B_2 < \infty, \quad \left\|\frac{\partial \Phi}{\partial M}\right\|_\infty = B_3 < \infty, \quad \left\|\frac{\partial \Phi}{\partial G_e}\right\|_\infty = B_4 < \infty,$$

$$\left\|\frac{\partial \Phi}{\partial G_l}\right\|_\infty = B_5 < \infty, \quad \left\|\frac{\partial \Phi}{\partial E_i}\right\|_\infty = B_6 < \infty, \quad \left\|\frac{\partial \Phi}{\partial E_a}\right\|_\infty = B_7 < \infty.$$

We would have established that the partial derivatives are bounded and hence the function $\Phi(x)$ defined by the right hand side of (8)–(14) is Lipschitzian. Now let x_1, x_2 be two arbitrary points in $\mathbb{R}_+^7$. Then define,

$$z(x_1, x_2; \theta) = \{x_1 + \theta(x_2 - x_1), \ 0 \leq \theta \leq 1\}.$$

Then, $z(x_1, x_2; \theta)$ is a line segment joining points x_1 and x_2 in $\mathbb{R}_+^7$ for $\theta \in [0, 1]$. Furthermore, $z(x_1, x_2; \theta)$ is a convex function and since $\mathbb{R}_+^7$ is a convex set, then $z(x_1, x_2; \theta) \in \mathbb{R}_+^7$ for each $\theta \in [0, 1]$.

Using the mean value theorem for differentiable functions in $\mathbb{R}_+^n$, one can show that

$$\|\Phi(x_1) - \Phi(x_2)\|_\infty = \|D_\Phi(c; x_1 - x_2)\|_\infty,$$

where c is the mean value point and D_Φ is the directional derivative of Φ at the point c in the direction of the vector $x_1 - x_2$. Using the expression for the directional derivative, as well as applying the triangle inequality and the Cauchy–Schwartz inequality, we see that

$$\|D_\Phi(z; x_1 - x_2)\|_\infty = \left\|\sum_{k=1}^7 \nabla\Phi_k(z) \cdot (x_1 - x_2)e_k\right\|_\infty$$

$$\leq \left\|\sum_{k=1}^7 \nabla\Phi_k(z)\right\|_\infty \|(x_1 - x_2)\|_\infty$$

$$\leq \sum_{k=1}^{7} \|\nabla\Phi_k(\mathbf{z})\|_\infty \|(\mathbf{x}_1 - \mathbf{x}_2)\|_\infty \leq \mathcal{L}\|(\mathbf{x}_1 - \mathbf{x}_2)\|_\infty,$$

for some constant $\mathcal{L} = 7\max\{B_1, B_2, B_3, B_4, B_5, B_6, B_7\}$ where the last inequality comes from the fact that each partial derivative of Φ is bounded and $\mathbf{e}_k$ is the kth unit vector in $\mathbb{R}_+^7$. Hence, there exists a constant $\mathcal{L} > 0$ such that

$$\|\Phi(\mathbf{x}_1) - \Phi(\mathbf{x}_2)\|_\infty \leq \mathcal{L}\|(\mathbf{x}_1 - \mathbf{x}_2)\|_\infty.$$

Hence, Φ is Lipschitz continuous and therefore, by the **Picard's existence and uniqueness theorem**, the system under study has a unique solution. $\square$

References

An G, Widness JA, Mock DM, Veng-Pedersen P (2016) A novel physiology-based mathematical model to estimate red blood cell lifespan in different human age groups. AAPS J 18(5):1182–1191

Anderson RM (1998) Complex dynamic behaviours in the interaction between parasite populations and the host's immune system. Int J Parasitol 28(4):551–566

Anderson RM, May RM (1979) Population biology of infectious diseases: Part I. Nature 280:361–367

Anderson RM, May RM (1991) Infectious diseases of humans: dynamics and control. Oxford University Press, Oxford

Anderson RM, May RM, Gupta S (1989) Non-linear phenomena in hostparasite interactions. Parasitology 99(S1):S59–S79

Aron JL (1983) Dynamics of acquired immunity boosted by exposure to infection. Math Biosci 64:249–253

Aron JL (1988a) Acquired immunity dependent upon exposure in an sirs epidemic model. Math Biosci 88:37–47

Aron JL (1988b) Mathematical modelling of immunity to malaria. Math Biosci 90(1):385–396

Augustine AD, Hall BF, Leitner WW, Mo AX, Wali Tonu M, Fauci Anthony S (2009) Niaid workshop on immunity to malaria: addressing immunological challenges. Nat Immunol 10(7):673–678

Baron S (1996) Medical microbiolgy—galveston (tx). University of Texas Medical Branch at Galveston

Baton LA, Ranford-Cartwright LC (2005) Spreading the seeds of million-murdering death: metamorphoses of malaria in the mosquito. Trends Parasitol 21(12):573–580

Bianconi E, Piovesan A, Facchin F, Beraudi A, Casadei Raffaella, Frabetti Flavia, Vitale Lorenza, Pelleri Maria Chiara, Tassani Simone, Piva Francesco et al (2013) An estimation of the number of cells in the human body. Ann Hum Biol 40(6):463–471

Bichara D, Cozic N, Iggidr A (2012) On the estimation of sequestered parasite population in falciparum malaria patients. [Research Report] INRIA, RR-8178:22

Bousema T, Drakeley C (2011) Epidemiology and infectivity of plasmodium falciparum and plasmodium vivax gametocytes in relation to malaria control and elimination. Clin Microbiol Rev 24(2):377–410

Bousema T, Sutherland CJ, Churcher TS, Mulder B, Gouagna Louis C, Riley Eleanor M, Targett Geoffrey AT, Drakeley Chris J (2011) Human immune responses that reduce the transmission of plasmodium falciparum in african populations. Int J Parasitol 41(3):293–300

Brännström BÅ, Sumpter DJT (2005) The role of competition and clustering in population dynamics. Proc R Soc B 272:2065–2072

Brookhaven National Labortory (BNL) (2017) 56 Facts About Blood and Blood Donation. https://www.bnl.gov/hr/blooddrive/56facts.asp. Accessed April 2017

Chiyaka C, Garira W, Dube S (2008) Modelling immune response and drug therapy in human malaria infection. Comput Math Method Med 9(2):143–163

Cowman AF, Berry D, Baum J (2012) The cellular and molecular basis for malaria parasite invasion of the human red blood cell. J Cell Biol 198(6):961–971

Cuomo MJ, Noel LB, White DB (2009) Diagnosing medical parasites: a public health officers guide to assisting laboratory and medical officers. Technical report, DTIC Document

Dean L, National Center for Biotechnology Information (U.S.) (2005) Blood groups and red cell antigens. NCBI

Eichner M, Diebner HH, Molineaux L, Collins WE, Jeffery GM, Dietz K (2001) Genesis, sequestration and survival of plasmodium falciparum gametocytes: parameter estimates from fitting a model to malariatherapy data. Trans R Soc Trop Med Hyg 95(5):497–501

Gardiner DL, Trenholme KR (2015) Plasmodium falciparum gametocytes: playing hide and seek. Ann Transl Med 3(4):45

Ginsburg H, Hoshen MB (2002) Is the development of falciparum malaria in the human host limited by the availability of uninfected erythrocytes? Malar J 1(1):18

Ginsburg H, Stein WD (1987) New permeability pathways induced by the malarial parasite in the membrane of its host erythrocyte: potential routes for targeting of drugs into infected cells. Biosci Rep 7(6):455–463

Gottlieb Y, Topaz O, Cohen LA, Yakov LD, Haber Tom, Morgenstern Abigail, Weiss Avital, Berman Karen Chait, Fibach Eitan, Meyron-Holtz Esther G (2012) Physiologically aged red blood cells undergo erythrophagocytosis in vivo but not in vitro. Haematologica 97(7):994–1002

Gravenor MB, Kwiatkowski D (1998) An analysis of the temperature effects of fever on the intra-host population dynamics of plasmodium falciparum. Parasitology 117(02):97–105

Gravenor MB, Lloyd AL (1998) Reply to: Models for the in-host dynamics of malaria revisited: errors in some basic models lead to large over-estimates of growth rates. Parasitology 117(05):409–410

Gurarie D, Karl S, Zimmerman PA, King CH, Pierre Timothy G St, Davis Timothy ME (2012) Mathematical modeling of malaria infection with innate and adaptive immunity in individuals and agent-based communities. PLoS One 7(3):e34040

Heffernan JM (2011) Mathematical immunology of infectious diseases. Math Popul Stud 18(2):47–54

Hellriegel B (1992) Modelling the immune response to malaria with ecological concepts: short-term behaviour against long-term equilibrium. Proc R Soc Lond B Biol Sci 250(1329):249–256

Hethcote HW, Stech HW, van den Driessche P (1982) Periodicity and stability in epidemic models: a survey. In: Busenberg S, Cooke KL (eds) Differential equations and applications in ecology, epidemics, and population problems. Academic Press, San Diego, pp 65–82

Hetzel C, Anderson RM (1996) The within-host cellular dynamics of bloodstage malaria: theoretical and experimental studies. Parasitology 113(01):25–38

Hoffman SL, Crutcher JM (2017) Malaria, Chapter 83. Medical Microbiology, Galveston (TX): University of Texas Medical Branch at Galveston, 4th ed, 1996. Accessed March 2017

Hollowell JG, Van Assendelft OW, Gunter EW, Lewis BG, Najjar M, Pfeiffer C (2005) Hematological and iron-related analytes-reference data for persons aged 1 year and over: United states, 1988–94. Vital Health Stat Ser 11 Data Natl Health Surv 247(247):1–156

Hoshen MB, Heinrich R, Stein WD, Ginsburg H (2000) Mathematical modelling of the within-host dynamics of plasmodium falciparum. Parasitology 121(03):227–235

Iggidr A, Kamgang J-C, Sallet G, Tewa J-J (2006) Global analysis of new malaria intrahost models with a competitive exclusion principle. SIAM J Appl Math 67(1):260–278

Ingemar N (1985) Lecture notes in biomathematics. Springer, Berlin

Janeway CA Jr, Travers P, Walport M, Shlomchik MJ (2001) Immunobiology: the immune system in health and disease, 5th edn. Garland Science, New York. Available from: https://www.ncbi.nlm.nih.gov/books/NBK10757/

Josling GA, Llinás M (2015) Sexual development in plasmodium parasites: knowing when it's time to commit. Nat Rev Microbiol 13(9):573–587

Kaushal DC, Carter R, Miller LH, Krishna G (1980) Gametocytogenesis by malaria parasites in continuous culture. Nature 286(5772):490–2

Kirk K (2001) Membrane transport in the malaria-infected erythrocyte. Physiol Rev 81(2):495–537

Kiszewski Anthony E (2010) Blocking plasmodium falciparum malaria transmission with drugs: the gametocytocidal and sporontocidal properties of current and prospective antimalarials. Pharmaceuticals 4(1):44–68

Kuehn A, Pradel G (2010) The coming-out of malaria gametocytes. BioMed Res Int 21(4):683–696

Landaw SA (1987) Factors that accelerate or retard red blood cell senescence. Blood Cells 14(1):47–67

Langhorne J (2006) Immunology and immunopathogenesis of malaria. Current topics in microbiology and immunology. Springer, Berlin

Langhorne J, Ndungu FM, Sponaas A-M, Marsh K (2008) Immunity to malaria: more questions than answers. Nat Immunol 9(7):725–732

Li Y, Ruan S, Xiao D (2011) The within-host dynamics of malaria infection with immune response. Math Biosci Eng 8(4):999–1018

McKenzie EF, Bossert WH (1997) The dynamics of plasmodium falciparum blood-stage infection. J Theor Biol 188(1):127–140

Mitri C, Thiery I, Bourgouin C, Paul REL (2009) Density-dependent impact of the human malaria parasite plasmodium falciparum gametocyte sex ratio on mosquito infection rates. Proc R Soc Lond B Biol Sci 276(1673):3721–3726

National Institute of Allergy and Infectious Diseases (NIAID) (2010) The life cycle of the malaria parasite. https://www.cdc.gov/malaria/about/biology/index.html. Accessed Jan 2018

Ngonghala CN, Ngwa GA, Teboh-Ewungkem MI (2012) Periodic oscillations and backward bifurcation in a model for the dynamics of malaria transmission. Math Biosci 240(1):45–62

Ngonghala CN, Teboh-Ewungkem MI, Ngwa GA (2015) Persistent oscillations and backward bifurcation in a malaria model with varying human and mosquito populations: implications for control. J Math Biol 70(7):1581–1622

Ngonghala CN, Teboh-Ewungkem MI, Ngwa GA (2016) Observance of period-doubling bifurcation and chaos in an autonomous ode model for malaria with vector demography. Theor Ecol 9(3):337–351

Ngwa CJ, de Rosa A, Thiago F, Pradel G (2017) The Biology of Malaria Gametocytes, chapter Current Topics in Malaria. InTech, 2016. Accessed March 2017

Ngwa GA, Teboh-Ewungkem MI (2016) A mathematical model with quarantine states for the dynamics of ebola virus disease in human populations. Comput Math Method Med, Vol 2016, Article ID 9352725, 93 pp

Okrinya A (2015) Mathematical modelling of malaria transmission and pathogenesis. PhD thesis, Loughborough University

Pearl R (1925) The biology of population growth. Alfred A. Knopf, New York

Perlmann P, Troye-Blomberg M (2002) Malaria immunology, chemical immunology and allergy. Karger, Basel

Rothman KJ, Greenland S, Lash TL (2008) Modern epidemiology. Lippincott Williams & Wilkins, Baltimore

Sackmann E (1995) Biological membranes architecture and function. Struct Dyn Membr 1:1–63

Shemin D, Rittenberg D (1946) The life span of the human red blood cell. J Biol Chem 166(2):627–636

Sinden RE (1982) Gametocytogenesis of plasmodium falciparum in vitro: an electron microscopic study. Parasitology 84(01):1–11

Sompayrac LM (2015) How the immune system works. John Wiley & Sons, New York

Talman AM, Domarle O, McKenzie FE, Ariey F, Robert Vincent (2004) Gametocytogenesis: the puberty of plasmodium falciparum. Malar J 3(1):24

Tavares JC (2013) Malaria. Colloquium series on integrated systems physiology: from molecule to function. Biota Publishing, Princeton

Teboh-Ewungkem MI, Wang M (2012) Male fecundity and optimal gametocyte sex ratios for plasmodium falciparum during incomplete fertilization. J Theor Biol 307:183–192

Teboh-Ewungkem MI, Yuster T (2010) A within-vector mathematical model of plasmodium falciparum and implications of incomplete fertilization on optimal gametocyte sex ratio. J Theor Biol 264(2):273–286

Teboh-Ewungkem MI, Yuster T (2016) Evolutionary implications for the determination of gametocyte sex ratios under fecundity variation for the malaria parasite. J Theor Biol 408:260–273

Teboh-Ewungkem MI, Podder CN, Gumel AB (2010) Mathematical study of the role of gametocytes and an imperfect vaccine on malaria transmission dynamics. Bull Math Biol 72(1):63–93

Teboh-Ewungkem MI, Ngwa GA, Ngonghala CN (2013) Models and proposals for malaria: a review. Math Popul Stud 20(2):57–81

Tewa J-J, Fokouop R, Mewoli B, Bowong S (2012) Mathematical analysis of a general class of ordinary differential equations coming from within-hosts models of malaria with immune effectors. Appl Math Comput 218(14):7347–7361

Tumwiine J, Luckhaus S, Mugisha JYT, Luboobi LS (2008) An age-structured mathematical model for the within host dynamics of malaria and the immune system. J Math Model Algor 7(1):79–97

Tumwiine J, Mugisha JYT, Luboobi LS (2008) On global stability of the intra-host dynamics of malaria and the immune system. J Math Anal Appl 341(2):855–869

Van den Driessche P, Watmough J (2002) Reproduction numbers and sub-threshold endemic equilibria for compartmental models of disease transmission. Math Biosci 180(1):29–48

Verhulst PF (1838) Notice sur la loi que la population suit dans son acroissement. Correspondence Mathématiwue et Physique 10:113–121

Wahlgren M, Perlmann P (1999) Malaria: molecular and clinical aspects. CRC Press, Boca Raton

Weekley C, Smith DS (2013) Malaria: the clinical basics. Global Health Education Consortium (GHEC)

WHO (2015) World malaria report 2015. World Health Organisisation Bulletine

Willekens FLA, Werre JM, Groenen-Döpp YAM, Roerdinkholder-Stoelwinder B, De Pauw Ben, Bosman Giel JCGM (2008) Erythrocyte vesiculation: a self-protective mechanism? Br J Haematol 141(4):549–556

Wongsrichanalai C, Barcus MJ, Muth S, Sutamihardja A, Wernsdorfer Walther H (2007) A review of malaria diagnostic tools: microscopy and rapid diagnostic test (rdt). Am J Trop Med Hyg 77(6 Suppl):119–127

World Health Organization and Center for Disease Control (2010) Basic malaria microscopy: tutor's guide. World Health Organization